

(NASA-CR-132500) X-RAY EMISSION FROM  
HIGH TEMPERATURE PLASMAS Final Technical  
Report (Old Dominion Univ. Research  
Foundation) 67 p HC \$3.75 CSCI 20I

N74-34199

Unclas  
G3/25 49647

## X-RAY EMISSION FROM HIGH TEMPERATURE PLASMAS

*A FINAL TECHNICAL REPORT*

*By*

Wynford L. Harries

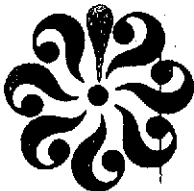


*Prepared for the*  
NATIONAL AERONAUTICS AND SPACE ADMINISTRATION  
Langley Research Center  
Hampton, Virginia 23665

*Under*  
Master Contract Agreement NAS1-11707  
Task Authorization NO. 23

*Submitted by the*  
Old Dominion University Research Foundation  
P.O. Box 6173  
Norfolk, Virginia 23508

July 1974



## CONTENTS

	<u>Page</u>
Final Technical Report on "X-ray Emission from High Temperature Plasmas" . . . . .	1
Bibliography. . . . .	4
Appendix A - Fine Structure of Hard X-ray Emission from a Plasma Focus Apparatus . . . . .	5
Figures . . . . .	10
Appendix B - Space and Time Resolved Observations of X-ray Production in a Plasma Focus Apparatus . . . . .	12
Figures . . . . .	17
Appendix C - Electron Dynamics in a Plasma Based on X-ray Measurements . . . . .	19
Bibliography . . . . .	31
Figures . . . . .	32
Appendix D - Spatial Distribution of the Electron Temperature in a Plasma Focus . . . . .	39
Bibliography. . . . .	46
Figures . . . . .	47
Appendix E - Use of Ross Filters to Measure the Energy Distribution of X-rays from Plasmas . . . . .	50
Bibliography . . . . .	58
Table . . . . .	59
Figures . . . . .	60

Final Technical Report  
NAS1-11707-23

X-ray Emission from High Temperature Plasmas

by  
W. L. Harries<sup>(1)</sup>

The investigation covered the period 30 June 73 to 30 June 74 and was carried out using the experimental facilities at NASA Langley Research Center.

The purpose of the work was to investigate the X-ray emission from Plasma Focus devices. Such devices emit X-rays up to 500 KeV and copious ( $10^9$  -  $10^{10}$  per pulse) neutrons. An understanding of the mechanisms involved would be helpful to explain solar flare phenomena, and could have applications for intense, short duration X-ray sources, possibly to pump X-ray lasers. Studies of such dense, high-temperature plasmas would also be of interest for controlled thermonuclear fusion applications.

Specifically the objectives were to determine the spatial and temporal variations of the X-ray emission from the plasma as well as obtain energy resolution. The results of the measurements are given in the appendices, and may be summarized as follows:

Triple pinhole cameras with filters showed that there may be three different mechanisms of X-ray emission from the plasma focus, (a) soft X-rays from the plasma, (b) hard X-rays from near the anode surface, (c) filamentary X-ray sources on the anode surface. The results were given at the Washington Meeting of the American Physical Society.<sup>(1)</sup> (Appendix A)

---

<sup>(1)</sup>Professor of Physics, Old Dominion University, Norfolk, VA 23508

A method of resolving X-ray production both in space and time showed that emission from the plasma occurred from 100 n sec prior to that from the anode, and that the latter continued for about 1  $\mu$  sec. The results were presented at the First International IEEE Conference at Knoxville, Tennessee<sup>(2)</sup> (Appendix B)

Measurements of emission vs angle showed different anisotropic behavior for low and high energy X-rays. The results were used to invoke the electron dynamics in the plasma, and it seems the electrons travel in a cone from the dense focus region towards the anode in near collisionless paths, gaining energy as they approach the anode (Appendix C).

By using filters and thermoluminescent detectors in 9 x 9 rasters in pinhole cameras, a two dimensional distribution of the electron temperature was obtained, with a value of about 10 KeV near the anode surface, dropping off to half value about 3 mm above it. (Appendix D)

The energy distribution of the X-rays could in principle be measured using Ross Filters, but before attempting the experiment an analysis of the signal to noise problems was made. It seems the measurement would require extremely high precision and a suggestion is made of overcoming this difficulty in the 67-89 KeV range (Appendix E).

Further work is required on the spatial distribution of electron temperature (Appendix D), especially to repeat the measurements viewing axially, which should then give a three dimensional distribution. The Ross Filter measurements (Appendix E) are to be undertaken possibly utilizing the space and time resolution method of Appendix B. In addition, preliminary attempts were made to obtain fast time response X-ray streak photographs using a lead collimator -NE102 scintillator arrangement. The light output was too low for an STL 500 camera using its normal lenses, and the scintillators will be tried against the photo cathode. These experiments will be undertaken

1 July 74 - 1 July 75 and a new grant NSG-1022 has been funded under the same title.

The author has greatly benefitted from the help and advice of J. H. Lee of Vanderbilt University, who is under NASA grant NGR-43-002-031, and D. R. McFarland of NASA. The single-pinhole picture, and the space-time resolved measurements used in the talks, were taken by them, and the author wishes to thank them most sincerely.

# BIBLIOGRAPHY

1. "Fine structure of hard X-ray Emission from a Plasma Focus Apparatus" W. L. Harries, J. H. Lee and D. R. McFarland, Bull Am. Phys Soc 19, 511, (1974).
2. "Space and Time Resolved Observations of X-ray Production in a Plasma Focus Apparatus" J. H. Lee, W. L. Harries and D. R. McFarland, First IEEE International Conference on Plasma Science, Knoxville, Tennessee, 15-17 May 1974, Paper 2C11.

Appendix A

Abstract Submitted

for the Washington, DC Meeting of the

American Physical Society

April 22-25, 1974

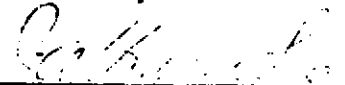
Physical Review  
Analytic Subject Index  
Number 35

Bulletin Subject Heading  
in which paper should be placed  
Plasma Physics, Experimental

Fine Structure of Hard X-Ray Emission From a Plasma-Focus Apparatus.<sup>+</sup> W. L. HARRIES, Old Dominion Univ., J. H. LEE, Vanderbilt Univ., and D. R. McFARLAND, NASA-Langley Research Center.--X rays from a 25-kJ plasma-focus apparatus were observed with pinhole cameras. The cameras consist of 0.4-mm diameter pinholes in 2-cm thick lead housing enclosing an x-ray intensifying screen at the image plane. Pictures recorded through thin aluminum foils or plastic sheets for x-ray energies  $E_\gamma < 15$  keV show distributed x-ray emissions from the focussed plasma and from the anode surface. However, when thick absorbers (2-mm thick Al or Pb, corresponding to  $E_\gamma > 15$  keV or  $E_\gamma > 150$  keV) are used, radial filamentary structure in the x-ray emission from the anode surface is revealed. Occasionally larger structures are observed in addition to the filaments. Possible mechanisms for the filamentary structure will be discussed.

<sup>+</sup>Work supported in part by NASA Grants NAS1-11707 and NGR 43-002-031

Submitted by

  
Signature of APS Member  
J. H. Lee

NASA-Langley Research Center

Mail Stop 160

Hampton, VA 23665

Washington Meeting April 22-26 1974 Paper EL12

FINE STRUCTURE OF HARD X-RAY EMISSION FROM A  
PLASMA-FOCUS APPARATUS

1. Introduction

This presentation is to report some new results on the X-ray emission from a plasma-focus device.

2. The plasma-focus device

The plasma-focus device consisted of a coaxial cylindrical cathode 25cm long and 10cm diameter and an internal anode of 5cm diameter - both of copper. It was energized by a 20 kV - 25 kJ capacitor bank.

3. Experimental method

The X-rays from the plasma focus were observed with pinhole cameras, with either single or triple pinholes, with filters of various thickness. The pinhole diameter was 0.4 mm minimum in a 2 cm lead housing, and the hole was tapered to get a full field of view. The pinholes were about 15 cm from the focus, and 15 cm behind them was placed an X-ray intensifying screen (DuPont Chronex, lightning) to give a 1:1 image. A Polaroid 3000 ASA film was placed immediately behind to get a contact print.

The multiple pinhole cameras gave adequate spatial resolution, and some measure of energy resolution, but as their pictures were integrated in time, therefore, a second experiment was carried out to introduce time resolution. We shall first discuss the time integrated pictures.

4. Experimental results

SLIDE 1 shows a typical pinhole photograph taken off axis through thin aluminum foil, placed over an aperture in the vacuum vessel. As is well-known, X-ray emission is observed from a column a few mm wide which extends downwards



into a cone. Intense emission seems to occur both at the plasma focus, and near to the anode surface. Similar end-on pictures confirm axial symmetry. The X-rays here would correspond to energies mostly near 15 keV.

To examine higher energy X-rays, pinhole cameras were aligned to observe through the vacuum vessel of 2 mm thick Al. SLIDE 2 shows the results. The lower picture had no lead filter; the middle was covered by 102 $\mu$ m of lead, and the top by 229 $\mu$ m of lead. The X-rays here correspond to what we may term "medium energy", or over 50 keV. It can be seen that emission is still visible from the plasma focus, but the greatest intensity comes from the anode surface. However, apparent now are sharp filaments of intense X-ray emission.

With no filters several long "fingers" appear to originate from the center of the anode. The lead filters, however, as in the previous slide, reduce the "fingers" considerably. Both an off-axis and end-on photo for the same discharge are recorded and the structure is apparent in both.

Similar pictures taken with two pinholes without filters, through the aluminum and viewed stereoscopically, indicated that the fingers were on or near the anode surface.

The next question of interest was to determine whether there was any difference in time between emission from the plasma, and from the anode. To determine this, we used a method which combined the spatial resolution of a pinhole camera, with the time resolution of photomultiplier tubes. The arrangement is shown in slide 3.

The pinhole camera imaged the X-rays on the intensifying screen. At p and e, two light pipes were placed, to cover an area of the image as shown, and the light signals directed to two photomultipliers, whose outputs were displayed on an oscilloscope versus time. The results show that emission from e occurs later than at p and increases for 500ns.

Next, Slide 4 shows the appearance of the anode after some hundred discharges.

The hole in the center was consistent with material being boiled away, rather than a pressure displacement because when a thin cap was placed over a hollow anode, there was little evidence of displacement of the lower surface, although the upper surface had been removed. Also, there was evidence of copper deposition on the aluminum vacuum chamber. The anode surface shows many ( $\sim 100$ ) radial filaments near the edges. Each filament is approximately 1 cm long and  $< 1$  mm thick.

## 5. Discussion

Emission in the focus occurs first when the electron and ion densities become high enough, and the electric fields have given the electrons sufficient energy. In the plasma focus, the target ions are mostly deuterium, with  $Z = 1$  and some copper impurity ions, which have high  $Z$  values. The pinhole pictures suggest emission from this region is mostly in the lower energy range of near 15 keV, and of lower intensity than near the anode.

As the electrons get accelerated towards the anode, they gain energy, and the pinhole pictures show that X-rays from near the anode are higher in energy. However, the emission time of X-rays from the anode is too long to be accounted by electrons ejected from the plasma focus.

The long emission time, and the appearance of the anode, suggest that the intense emission from the anode region continues during vaporization of the copper, with subsequent ionization in the plasma to high  $Z$  ions. Furthermore, the electrons are forming filaments rather than an uniform distribution. This tends to support the existence of microstructures in the plasma focus itself.

In conclusion, Slide 5, it seems that X-ray emission in the plasma focus consisted of:

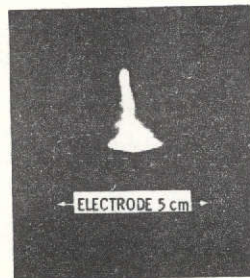
(1) Soft X-ray emission from the compressed plasma region mostly due to deuterium ions with  $Z = 1$

(2) Hard X-ray emission from the solid copper anode

(3) Filamentary X-ray sources on the anode surface.

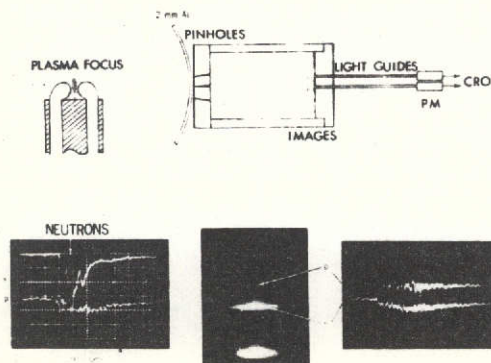
(2) & (3) have a longer emission time ( $>500\text{ns}$ ) long after the plasma focus X-ray emission ( $<100\text{ns}$ ) is ended. This last evidence can be taken as the result of a non-thermal component of plasma electrons associated with the plasma focus formation.

X-RAY PINHOLE CAMERA PHOTOGRAPH  
LOW ENERGY ( $\sim 15$  keV) THROUGH AZ FOIL



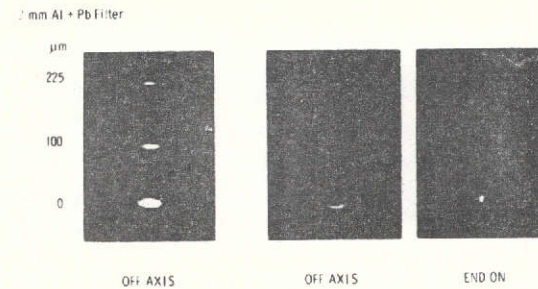
SLIDE 1

SPACE-TIME RESOLVED X-RAY MEASUREMENT

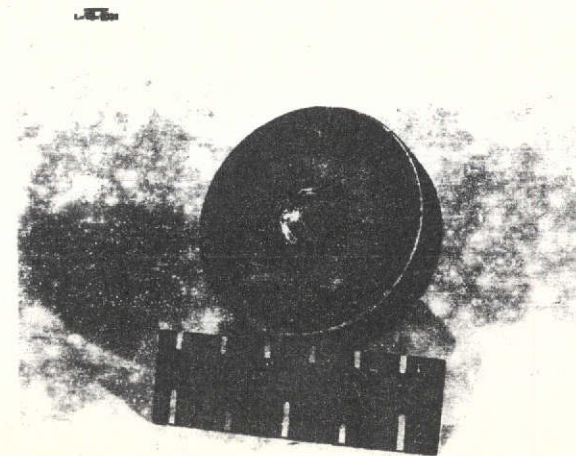


SLIDE 3

X-RAY PINHOLE CAMERA PHOTOGRAPHS



SLIDE 2



SLIDE 4

REPRODUCIBILITY OF THE  
ORIGINAL PAGE IS POOR

X-RAY EMISSION FROM PLASMA FOCUS

- (1) Soft X-ray emission from the focused plasma
- (2) Hard X-ray emission from the anode surface
- (3) Filamentary X-ray sources on the anode surface

SLIDE 5

REPRODUCIBILITY OF THE  
ORIGINAL PAGE IS POOR

May 15-17, 1974 Knoxville, Tennessee Paper 2C11

SPACE AND TIME-RESOLVED OBSERVATIONS OF X-RAY PRODUCTION

IN A PLASMA-FOCUS APPARATUS<sup>+</sup>

by J. H. Lee, Vanderbilt University, Nashville, TN 37235,  
W. L. Harries, Old Dominion University, Norfolk, VA 23508,  
and

D. R. McFarland, NASA-Langley Research Center, Hampton, VA 23665

Abstract

Space and time-resolved information on the x-ray production in a plasma-focus apparatus is obtained by monitoring the fluorescence in the image plane of an x-ray pinhole camera at different positions with a light-guide-photomultiplier system. The plasma focus is produced with a pair of coaxial electrodes energized by a 20 kV-25kJ capacitor bank. The density and temperature of the plasma focus are  $n_e \approx 10^{20}/\text{cm}^3$  and  $T_e \approx 5$  keV, respectively. Intense bursts of x-rays (up to 500 keV)<sup>1</sup> and neutrons ( $\approx 10^{10}$  per focus formation) are produced with deuterium as the filling gas.<sup>2</sup> Part of the intense x-ray emission is caused by a strong beam of particles directed toward the center electrode (anode). To separate and identify various sources of x-ray production in the apparatus, both space and time-resolved observations are necessary. The present system combines the space resolution of a pinhole camera with the fast time resolution of a light-guide-photomultiplier arrangement. Here, the pinhole diameter was 0.4 mm and the image-to-object ratio 1:1, forming an image about 3 cm across. The space resolution of the system is determined by the area of the screen observed and the time resolution is determined by the photomultiplier tube and the electronics (about 20 ns). The location of the light guides is determined by first taking an x-ray image of the plasma focus on a polaroid film. Images representing the plasma and the anode are then viewed through 3-mm diameter holes and the light guides are directed from these holes to two identical photomultiplier channels recording simultaneously on a dual-beam oscilloscope. Specially constructed hollow aluminum cylinders were used as guides because commercially available fiberglass light pipes were found to be sensitive to x-rays. Results on the onset times and intensity variations of x-rays from the plasma as compared to those from the anode will be presented. This method is much simpler, less expensive, and yet more sensitive than an x-ray image converter camera.

<sup>+</sup> Work supported in part by NASA Grants NGR 43-002-031 and NAS1-11707

1. J.H.Lee, D.S.Loebbaka, and C.E.Roos, Plasma Physics, 13, 347 (1971)
2. J.H.Lee, L.P.Shomo, M.D.Williams, and H.Hermansdorfer, Phys. Fluids 14, 2217 (1971)

## SPACE AND TIME-RESOLVED OBSERVATIONS OF X-RAY PRODUCTION IN A PLASMA-FOCUS APPARATUS

X-ray production in a plasma-focus apparatus is a rather complex phenomenon, and time and space resolved information is necessary for better understanding of its mechanism. A light guide-photomultiplier system combined with pinhole cameras were used to obtain such information with the NASA-Langley plasma-focus apparatus.

The first slide shows a schematic of the apparatus. A pair of coaxial electrodes is connected to a 20 kV-25 kJ capacitor bank. When the capacitor bank is fired by trigatron switches, the initial breakdown takes place over the insulator and a current sheet is formed.  $\mathbf{J} \times \mathbf{B}$  force, then, accelerates this mushroom-shaped current sheet toward the ends of the electrodes, where the current sheet strongly collapses toward the axis of the electrodes. The impedance of the apparatus and the pressure of working gas are so adjusted that the peak current flows at the time of the collapse. A small volume of extremely hot and dense plasma, called a plasma focus, is formed over the center electrode. When deuterium is used as the working gas, nuclear fusions take place in the plasma and about  $10^{10}$  neutrons per pulse are emitted.

The next slide lists results of some observations made on the plasma focus.

The next slide shows the x-ray image of the plasma focus taken through 100  $\mu\text{m}$  of Al foil. X-rays are emitted not only from the focus but distributed down to the surface of the center electrode.

The next slide shows the arrangement of two pinhole cameras. Each camera had 3-400- $\mu\text{m}$  diameter pinholes so that different absorbers can be used simultaneously. We used 100 and 225  $\mu\text{m}$  of lead foils in addition to the 2-mm thick aluminum wall of the vacuum chamber.

Crude energy resolutions, about 15, 50 and 100 keV, are obtained with this arrangement. The magnification of the camera is unity, and an x-ray intensifying screen is used in contact with a polaroid film to record the x-ray images.

The next slide shows the pictures made with these cameras. Unlike the x-ray images shown in the earlier slide, we now find fine structures in these hard x-ray pictures. The lower pictures were taken without a lead filter, the middle was covered by 100  $\mu\text{m}$  of lead, and the top by 225  $\mu\text{m}$  of lead, as shown in the previous slide.

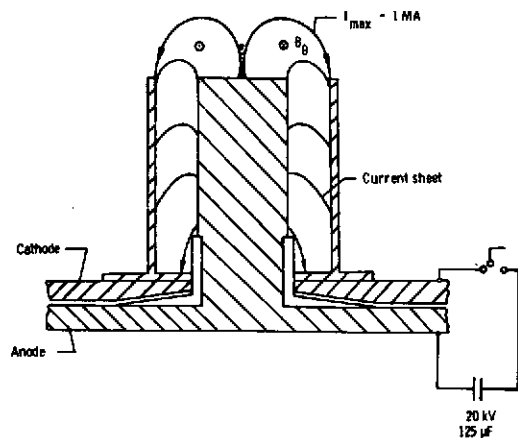
It can be seen that x-ray emission is still visible from the plasma focus, but the greatest intensity comes from the anode surface. Furthermore, apparent now are sharp filaments of intense x-ray sources. The first picture even has a few long "finger" shaped sources. These appear to originate from the axis of the center electrode. It is still visible in the middle picture taken through 100  $\mu\text{m}$  of lead filter, indicating x-ray energies of greater than 50 keV are present. The second and third pictures were taken on and off axis simultaneously. These show that the filaments are radially oriented, approximately one centimeter long, and located on or near the surface of the electrode. Since pinhole camera pictures only provide time integrated information, we devised a method which combined the space resolution of a pinhole camera with the time resolution of photomultiplier-oscilloscope system. The arrangement is shown in the next slide.



To monitor the intensity variations of the x-ray image, two light guides made of polished aluminum tubes are placed behind the intensifying screen as shown in the picture. The commercially available fiberglass light pipes were not suitable because it was found they become fluorescent from the x-rays and neutrons. P and e denote image points corresponding to the plasma focus and the electrode, respectively. The light signals from these points are directed to two photomultipliers, whose outputs are displayed on an oscilloscope. These are shown in the pictures below. We see that x-ray emission from the electrode occurs approximately 20 ns later than x-ray emission from the plasma focus itself. Also, the x-ray emission from the electrode continues for more than 500 ns as indicated by increase of light signals on the lower trace. This indicates that the hard x-ray emission from the electrode surface continues beyond the plasma focus lifetime, and well into during vaporization of copper, the electrode material. An explanation with a simple model, that x-ray emission from the electrode surface is only due to bombardment of electrons ejected from the plasma focus, is not sufficient to account for these results. For a 50 keV electron, the time needed to reach the electrode surface from the focus position, 1.5 cm above, is only a fraction of a nanosecond, and x-ray emission is expected to last only for the lifetime of the focus, contrary to the actual observation for more than 500 ns. This discrepancy, together with the observation of filamentation, may be important for understanding of mechanism for plasma-focus formation.

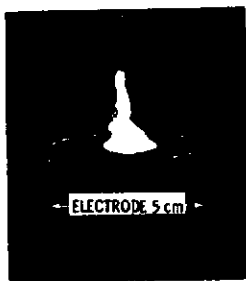
Our method could be extended to map any point in the area of x-ray image displayed on the fast scintillation material. A nanosecond time

resolution and sub-millimeter space resolution could be obtained without difficulty since high gain photomultipliers are available commercially. This method is much simpler, less expensive, and yet more sensitive than an expensive x-ray image-converter camera-collimator system.



SLIDE 1

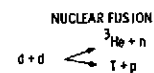
X-RAY PINHOLE CAMERA PHOTOGRAPH  
LOW ENERGY (1-15 keV) THROUGH Al FOIL



SLIDE 3

# THERMAL

$T_0$  3 keV  
 $T_1$  8 keV  
 $n_1 = n_2$   $5 \times 10^{19} \text{ cm}^{-3}$   
 SIZE 1 mm dia.  
 10 mm long

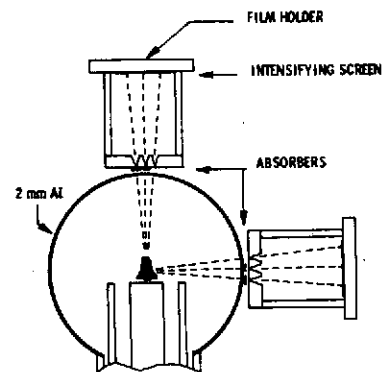


NON-THERMAL  
 $E_0$  up to 500 keV  
 (by hard x-rays)  
 $E_1$  up to 100 keV  
 (by neutron energy)

NEUTRON EMISSION  $10^{10}$  PER PULSE  
 PULSE DURATION 100 ns

SLIDE 2

# TRIPLE PINHOLE CAMERAS



SLIDE 4

REPRODUCIBILITY OF THE  
ORIGINAL PAGE IS POOR

REPLACEMENT QUALITY OF THE  
ORIGINAL PAGE IS POOR

X-RAY PINHOLE CAMERA PHOTOGRAPHS

2 mm Al + Pb Filter

$\mu\text{m}$

225

100

0



OFF AXIS



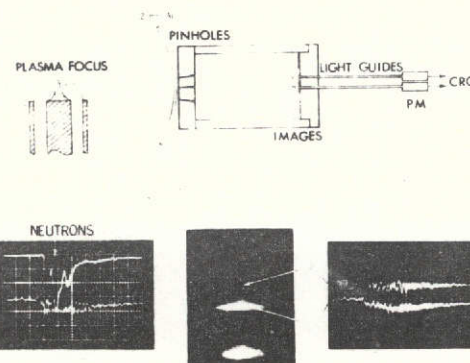
OFF AXIS



END ON

SLIDE 5

SPACE-TIME RESOLVED X-RAY MEASUREMENT



SLIDE 6

ELECTRON DYNAMICS  
IN A PLASMA BASED ON X-RAY MEASUREMENTS

Summary

The intensity of X-rays from a Plasma Focus was measured as a function of angle  $\theta$  from the axis of symmetry, for  $0 < \theta < \pi/2$  and for  $\theta = \pi$ , or behind the anode, by using thermoluminescent detectors. In addition energy analysis was performed by using filters. Considerable anisotropy was revealed; the polar diagram of medium energy ( $\approx 20$  KeV) X-rays resembled a cardioid, but that for higher energy ( $\approx 100$  KeV) showed a lobe into the anode, with a forward to back ratio of about 50. This indicates the plasma was near collisionless with runaway relativistic electrons, in severely anisotropic velocity distributions. By considering Bremsstrahlung emission from relativistic electrons, an explanation is suggested for the radiation patterns. Conversely, the patterns are used to invoke electron trajectories, which appear consistent with results of multiple pinhole energy-analysing cameras.

## I. Introduction

The investigation of dense, high temperature plasmas is of interest both in astrophysics, and in the controlled thermonuclear fusion program. Such plasmas can be obtained from plasma focus devices, sufficiently dense and energetic to emit neutrons and X-rays<sup>1-9</sup>.

The purpose of this investigation was to study the Bremsstrahlung X-ray from a plasma focus. Studies of the angular dependence of the intensity have been made previously and showed that the emission was not isotropic.<sup>9</sup> The results are confirmed here, and considerably extended by a different technique. In addition, we find a different behavior for low energy ( $\approx 20$  KeV) and high energy ( $\approx 100$  KeV) emission.

Section II describes the experimental method, and results. In Section III, an explanation is offered for the experimental behavior and conversely, the results are invoked to yield information on the particle dynamics.

## II. Experimental Method

### A. Plasma-focus device

The plasma-focus device<sup>5,6</sup> consisted of a coaxial cylindrical cathode 23 cm long and 10 cm diameter and an internal anode of 5 cm diameter--both of copper (Fig. 1). They were enclosed in an aluminum sphere of 2 mm wall thickness and 30 cm diameter. The gas was deuterium at about 7 torr. A 125 $\mu$ F capacitor bank, charged to 20 kV provided 25 kJ energy. During the "focus" stage, the plasmas were compressed into a volume  $\sim 10^{-2}$  cm<sup>3</sup>, with densities

$10^{19}\text{cm}^{-3}$ , and electron temperatures of several kilovolts. Copious neutrons  $10^{10}$  per focus were obtained as well as X-rays of over 100 keV<sup>8,9</sup>. Here, we shall discuss only the X-ray emission.

#### B. Experimental Measurements.

Numerous diagnostics, such as X-ray and neutron scintillator-photomultiplier detectors and image converter cameras in both streak and framing modes were used<sup>6</sup>, but, the main results here are based on two techniques, namely, the use of pinhole cameras and secondly, thermoluminescent detectors.

The pinhole cameras were designed with three pinholes to provide both spatial information on the X-ray emission, and also energy resolution vs position. Each pinhole was tapered and of 0.4 mm diameter (minimum) in a 2 cm thick lead housing. One pinhole observed through the 2 mm thick aluminum vessel, and the other two were shielded by lead filters of various thickness in addition. The pinholes were about 15 cm from the focus, and 15 cm behind them was placed an X-ray intensifying screen (DuPont Chronex Lightning) to give a 1:1 image. A Polaroid 3000 ASA film was placed immediately behind the screen to get a contact print. The film was sufficiently sensitive to easily record a single shot, and gave better detail than Polaroid 10,000 ASA film.

Fig. 2 shows triple-pinhole camera pictures of a typical discharge observed through the vessel at  $\theta = 80^\circ$ , with the middle and upper pictures taken through filters of 102 and 225  $\mu\text{m}$  of lead in addition. The spatial resolution is adequate, and X-ray emission is visible from the plasma about 2 cm above the anode, from a region about 1 mm wide at the top extending downwards in a cone.

The intensity from near the anode surface is many times greater than from the plasma. By comparing the ratio of the intensities in the three pictures, we see that the filters reduced the intensity of emission from the plasma to a greater extent than that from the anode surface, a fact we shall use later to invoke a qualitative comparison of the X-ray energy, in these regions.

The thermoluminescent detectors<sup>10</sup> (TLD) can give quantitative estimates of the intensity of the time integrated X-ray emission. These are small squares, 1/8" x 1/8" x 1/32" of various insulating crystals, which when irradiated with X-rays, can store some of the energy in metastable states. Some of this energy can be recovered later as visible photons if the material is heated. A commercially available analyser<sup>11</sup> was used to measure the incident radiation. Moreover, the dynamic range of the analyser ( $\approx 10^6$ ) enables the detectors to be used for a single pulse or left on the apparatus to integrate the effects of many pulses. We investigated several types of detectors--Harshaw type 700, which measured x rays only, but were too insensitive, type 600 which measured neutrons and type 400 which measured both.

A comparison of the contribution from X rays versus neutrons was made by using filters of lead with and without Boron filled polyethylene, to trap neutrons. The results indicated that the TLD 400 output signal was approximately proportional to the X ray irradiation. Also, 18 such detectors exposed simultaneously gave outputs within  $\pm 5\%$ . Their small size enabled accurate measurements to be made vs angle  $\theta$  from the axis.



Our first measurements for  $0 < \theta < \pi/2$  were made with the detectors placed roughly every  $15^\circ$  outside the aluminum sphere as in Figure 1D. (The anode surface was 2.5cm below the center of the sphere). For  $\pi/2 \leq \theta < \pi$  the anode and cathode shielded the detector from radiation emanating from near the anode surface. We did not attempt intermediate angles between  $\pi/2$  and  $\pi$ , but obtained readings for  $\theta = \pi$  by placing detectors inside a hole in the anode at B. Thus, the small size of the detectors proved advantageous, as they could operate inside as well as outside the vacuum vessel.

To normalize the reading at B with readings at D, it was necessary to interpose the same material. The anode was usually copper and first a copper cap was placed at H and detectors placed at A inside the vessel at  $\theta = 75^\circ$  behind a similar copper shield. Simultaneously, the readings at  $0^\circ$  were taken with plate C of copper, and also through the vessel at  $\theta = 75^\circ$ . In a further experiment, the plates at H and C were made of aluminum, and readings taken simultaneously at D. The plates were all 2 mm thick, similar to the vacuum wall, and the distances of the detectors from the focus approximately 15 cm.

The detectors were supported on paper inside lead holders and shielded from the plasma and any vaporized metals. During a run, the apparatus became hot and the detectors had to be thermally insulated to prevent loss of luminescence. The holders at C & D were kept about 0.5 cm away from the vacuum vessel and that at A from its shield by three screws, whilst those at B were separated

from the copper by polystyrene. Comparison of measurements made inside the vessel, and outside where there was adequate cooling, indicate that the detectors lost hardly any of their response due to heating.

In addition to measuring vs  $\theta$ , we obtained energy resolution by using filters. All the holders except that at B held eighteen detectors in six sets of three, with the first set observing the plasma through only (paper and) the shield/vacuum vessel and the other five sets, in addition, observing through different lead filters of thickness 102, 203, 304, 508 and 762  $\mu\text{m}$ , respectively. Similar filters were used at B, but only one detector per filter was possible due to lack of space.

### III Results

The X-ray emissions from about 65 focuses were superimposed on the thermoluminescent detectors through the vessel wall, and are recorded in Fig. 3, as readings of intensity, in units of nano-Coulombs vs filter thickness for different  $\theta$ . Values for  $\theta = 0$  and  $\pi/2$  are not shown; for the former the plate was eroded, and the detectors for the latter were cut off by the cathode. The values shown are the average of three readings and the intensities show slight increases with  $\theta$ , up to  $62^\circ$ .

Readings with detectors at A B C & D (Fig 1) were then made with the anode surface (plate H) and the shields A and C of aluminum, and also with all three of copper. There were no great differences in the plasma behavior whether copper or aluminum were used. Results for aluminum (Fig 4) with about 20 focuses

superimposed (less than previously, to prevent erosion), show that the curves for the detectors at A and D resemble Fig. 3. The curve for the detectors at C is lower for all filters, whilst for those at B, it is higher. The ratio between curves B and C is about 2 with no filter, and about 40 for the thickest filter. Results with copper were similar and the ratio of B to C was about 5 for no filter and about 40 with the thickest filter. The values at A were intermediate, as for aluminum, and were up to about 4 times higher than C.

By normalizing B and C to the values at D or A at  $75^\circ$ , we may estimate the values for  $\theta = 0$  and  $\pi$ , and draw Polar diagrams of X-ray intensity (Fig 5a and b). Values for 0 and  $762 \mu\text{m}$  lead + 2 mm aluminum are shown. All three readings for each  $\theta$  are shown and the circles are for aluminum at A, H and C in Fig 1. The pattern in Fig 5(a) confirms previous results<sup>9</sup> for  $0 < \theta < \pi/2$ , showing reduced intensity for  $\theta = 0$  and assuming the curve is drawn correctly to the extra point at  $\theta = \pi$  resembles a cardioid. The pattern in (b) is greatly different--a forward lobe about 50 times greater than the backwards or sideways signal is evident. The polar diagrams for intermediate filters would be intermediate between a cardioid and a narrow lobe as is evident from Fig. 4.

Similar polar diagrams were obtained with copper at A, H, and C in Fig. 1. However, with no filter, the diagram showed a slightly downward oriented lobe, and is indicated with the two crosses in Fig 5(a), normalized to the signal at  $\theta = 45^\circ$ . With the  $762 \mu\text{m}$  filter, a pronounced lobe was observed with a forward-back ratio of from 20 to 40.

### III. Discussion.

From the X-ray picture (Fig 2) it can be seen that the region of X-ray emission extends from the focus in a cone to the anode. The intensity depends on the plasma density, the value of  $Z$  for the ions (sensitive to impurities) and the electron energy.

The plasma density in the focus was about  $10^{19}\text{cm}^{-3}$ , and we would expect the density to fall by a factor of about a hundred as we approach the anode. In the plasma, the intensity of emission would be proportional to the product of electron and ion densities  $n_e n_i$  or  $n_e^2$ , while that from the anode would depend on  $n_e n_t$ , where  $n_t \approx 10^{22}$  is the density of copper atoms in the anode. The high  $Z$  of copper should also contribute to the observed more intense radiation from the anode. More important, the emission is extremely sensitive to electron energy, and a single pinhole picture or thermoluminescent detector reading cannot differentiate between particle density and electron energy.

The lead filters gave a measure of energy selectivity. In the case of the pinhole pictures, the aluminum vessel alone transmitted X-rays of  $\gtrsim 15$  KeV while the 102 and 225  $\mu\text{m}$  filters transmitted energies  $\gtrsim 20$  and  $\gtrsim 30$  KeV, respectively. The ratio of the intensities for the same point in the plasma recorded through two different filters, gives a qualitative estimate of the X-ray energy--the higher the energy, the more will the ratio approach unity. We may compare the electron energy at two different points by estimating such ratios. Differences in particle density at the two points do not matter as we are using ratios. In Fig 2, the Bremsstrahlung from the plasma has been greatly reduced by the

102  $\mu\text{m}$  filter, but the emission from the anode region is still transmitted through the 225  $\mu\text{m}$  filter. The problem of film saturation and linearity enter here, although we may avoid the former by observing grey regions on the anode. Qualitatively it seems the electron energy is higher near the anode than in the focus region.

In the case of the thermoluminescent detectors, we used both 2 mm aluminum and 2 mm copper in conjunction with various lead filters: with 2 mm of aluminum alone, X-rays of  $> 15$  KeV are transmitted, but only those over 50 KeV are observed with 762  $\mu\text{m}$  of lead, in addition. If copper is substituted for aluminum, then as its absorption coefficient is higher, X-rays of  $> 30$  KeV would be transmitted with no filter, and  $> 60$  KeV with a 762  $\mu\text{m}$  lead filter. Therefore, Fig 5(a) corresponds to "medium" energies,  $> 15$  KeV for aluminum, and  $> 30$  KeV for copper, while Fig 5(b) corresponds to energies of order 100 KeV, indicating electrons of this energy existed in the plasma.

We next examine the plasma parameters. For electrons of these energies, the plasma would be near collisionless. Even at 5 KeV (a number quoted as electron temperature in a focus<sup>8</sup>) the coulomb cross sections of ions are of order  $10^{-20}$   $\text{cm}^2$ , and assuming  $n_e \sim 10^{19} \text{cm}^{-3}$ , the mean free paths of electrons would be about 10 cm, much larger than the plasma dimensions.

The electrons causing the X-rays would be in the high energy tail of the distribution. The observation of X-rays of over 50 KeV indicates voltage differences of this amount must occur, which if applied over distances of order 1 cm, imply fields of  $5 \times 10^4$  V/cm.

Then applying the criterion of Dreicer<sup>12</sup>, all electrons over 200 eV should run away. Further, such electric fields would make the electron velocity distribution severely anisotropic, and the electrons relativistic.

However, all of the electrons would not be swept out of the plasma--the observed "containment" time was of order  $10^{-7}$  sec<sup>9</sup>. Assuming  $n_e=10^{19}\text{cm}^{-3}$ ,  $T_e=5\text{KeV}$ , the Debye Length would be about  $10^{-5}\text{cm}$ , and the number of particles in a Debye Sphere about  $10^4$ , the  $90^\circ$  deflection time for electrons by ions,  $T_D=10^{-9}$  sec, as well as the electron-electron equipartition time. The electron-ion equipartition time would be several  $\mu\text{s}$ ,--longer than the containment time, so we would expect electrons and ions to gain energy from the electric field, but little energy would be handed from electrons to the ions.

In summary, we would expect a dense, electron-relativistic near-collisionless Plasma, with the electron velocity distribution anisotropic. (However, there might be particle deflections from the strong electric and magnetic fields present.)

The anisotropy of the Bremsstrahlung intensity vs  $\theta$  indicates ordered motion of the electrons, and we assume that they travel from the high density region in approximately straight lines, consistent with a "collisionless" plasma. The pinhole pictures also indicate that low energy Bremsstrahlung are emitted from the focus region and higher energies from near the anode, suggesting the electrons gain energy in proceeding to the anode. The fact that the electric fields are thus directed is not obvious, as violent voltage fluctuations appear during a focus.

Although care must be taken in interpreting the pinhole pictures, the region of emission implies that the trajectories of the high energy electrons lie in a cone and Fig 6(b) shows such trajectories qualitatively.

The emission of Bramsstrahlung from a directed beam of electrons is well-known and the intensity  $\Pi(\phi)$  from one electron per unit solid angle per unit time is given by<sup>13</sup>

$$\Pi(\phi) = \frac{q^2 \{a^2\} \sin^2 \theta}{16\pi^2 \epsilon_0 c^3 (1 - \beta \cos \theta)^5} \quad (1)$$

Here  $q$  is the charge of the electron,  $a$  the value of the vector acceleration,  $\epsilon_0$  the dielectric constant of free space,  $c$  the velocity of light and  $\phi$  the angle of emission relative to the forward direction of the electron. The expression includes relativistic effects and  $\beta$  is the usual  $v/c$ . For convenience, the radiation patterns are shown in Fig 6(a), for different electron energies. As  $\beta \rightarrow 0$  there is no radiation forward or backward, but as  $\beta$  increases the radiated power is directed predominantly in the forward direction.

Then the measured intensity at any given  $\theta$  would be the sum of patterns similar to Fig 6(a) from electrons in a cone whose velocity vectors are at any angle up to  $\alpha$  relative to the axis of symmetry of the apparatus (Fig 6b). The intensity pattern vs  $\theta$  at energies  $\approx 20$  KeV would then resemble a cardioid as in Fig 5(a) and at energies  $\approx 100$  KeV would give a forward lobe as in Fig 5(b). The pattern for copper ( $\approx 30$ KeV) would be intermediate, as observed. It should be remembered that the measured intensity depends not only on  $\Pi(\phi)$  relative to a given direction, but also the number of electrons in that direction and their energies, which we have not measured.

The fact that part of the emission comes from the solid target is consistent with the argument. Although the electrons might suffer large angle deflections in the solid, the emission of high energy Bremsstrahlung is mostly due to first deflections, and thereafter the electron energy is too low for further high energy emission. Comparison of Fig 5(b) with Fig 6(a) suggests values of  $B \approx 0.5$  or electrons of energy  $\approx 100\text{KeV}$ , consistent with the transmission data of the lead filters.

#### V. Conclusions

Measurements of the intensity of X-rays from a Plasma Focus show that the emission is anisotropic, the more so for higher energies ( $\approx 100\text{ KeV}$ ) than for lower, ( $\approx 20\text{KeV}$ ). Consideration of the plasma parameters show that it should be near collisionless, and that most of the electrons should be in a run away condition. From the radiation pattern of relativistic electrons, a qualitative picture is obtained which, explains the radiation patterns. The picture indicates that the electron velocity vectors lie in a cone between the point of focus in the plasma and the anode and that their energies should be up to  $100\text{ KeV}$ , consistent with observations of transmission through filters using multiple pinhole cameras and thermoluminescent sensors.

#### ACKNOWLEDGEMENTS

The authors would like to thank Dr. Frank Hohl and Mr. George Wood for their interest and support. The work was carried out at the National Aeronautic and Space Administration Research Center, Langley, under grants NAS1-11707-23 and NGR 43-002-034.



# BIBLIOGRAPHY

1. D. P. Petrov, N. V. Filippov, T. I. Filippova and V. A. Khrabrob, in "Plasma Physics and the Problems of Controlled Thermonuclear Reactions" (Pergamon, London, 1960), Vol IV, p. 198.
2. N. V. Filippov, T. I. Filippova, and V. P. Vinogradov, Nucl. Fusion Suppl. 2, 566 (1962).
3. J. W. Mather, Bull. Am. Phys. Soc. 8, 177(1963); 9, 339(1964).
4. J. W. Mather, Phys. Fluids Suppl. 7, S28(1964).
5. E. H. Beckner, J.A.P. 37, 4944(1967).
6. E. H. Beckner, E. J. Clothiaux and D. R. Smith, Phys. Fluids 12, 253 (1969).
7. H. L. L. van Paassen, R. H. Vandre and R. S. White, Phys Fluids 13, 2606(1970).
8. J. H. Lee, L. P. Shomo, M. D. Williams, and H. Hermansdorper, Phys. Fluids 14, 2217(1971).
9. H. W. Jalufka and J. H. Lee, Phys Fluids 15, 1954(1972).
10. J. R. Cameron, N. Suntharalingam and G. N. Kenney, "Thermoluminescent Dosimetry" (Wisconsin Press) 1968.
11. The Equipment used was manufactured by the Harshaw Chemical Company, 1945 E 97 St., Cleveland, Ohio 44106.
12. H. Drieger, Phys. Rev. 115 238 (1959).
13. See for example, R. B. Leighton, "Principles of Modern Physics" McGraw Hill 1959, p. 413.



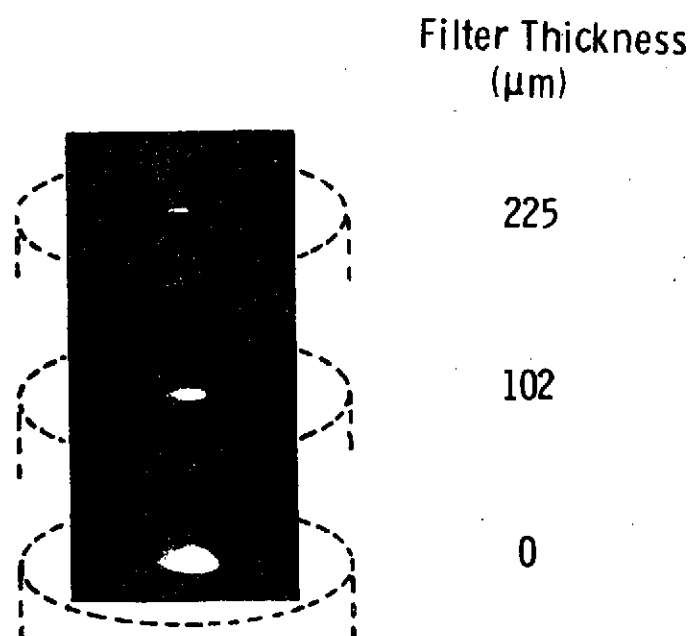


Fig. 2. Triple pinhole camera pictures of X-rays from the plasma focus taken through the aluminum vacuum vessel and various lead filters.

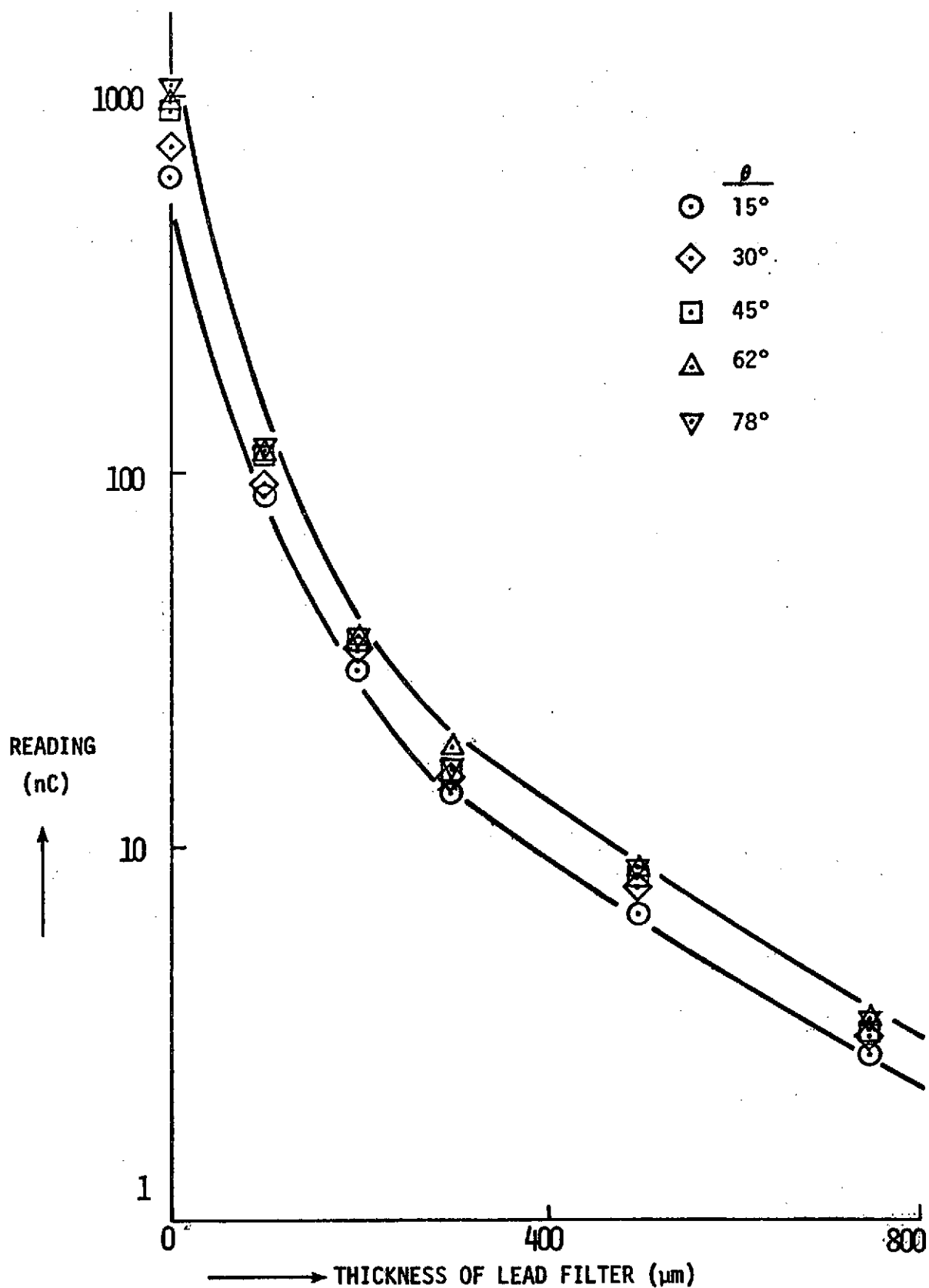


Figure 3. Plot of TLD Readings vs Thickness of Lead Filters, and Various Values of  $\theta$ . The Readings Were Taken Through the 2 mm Aluminum Vessel.

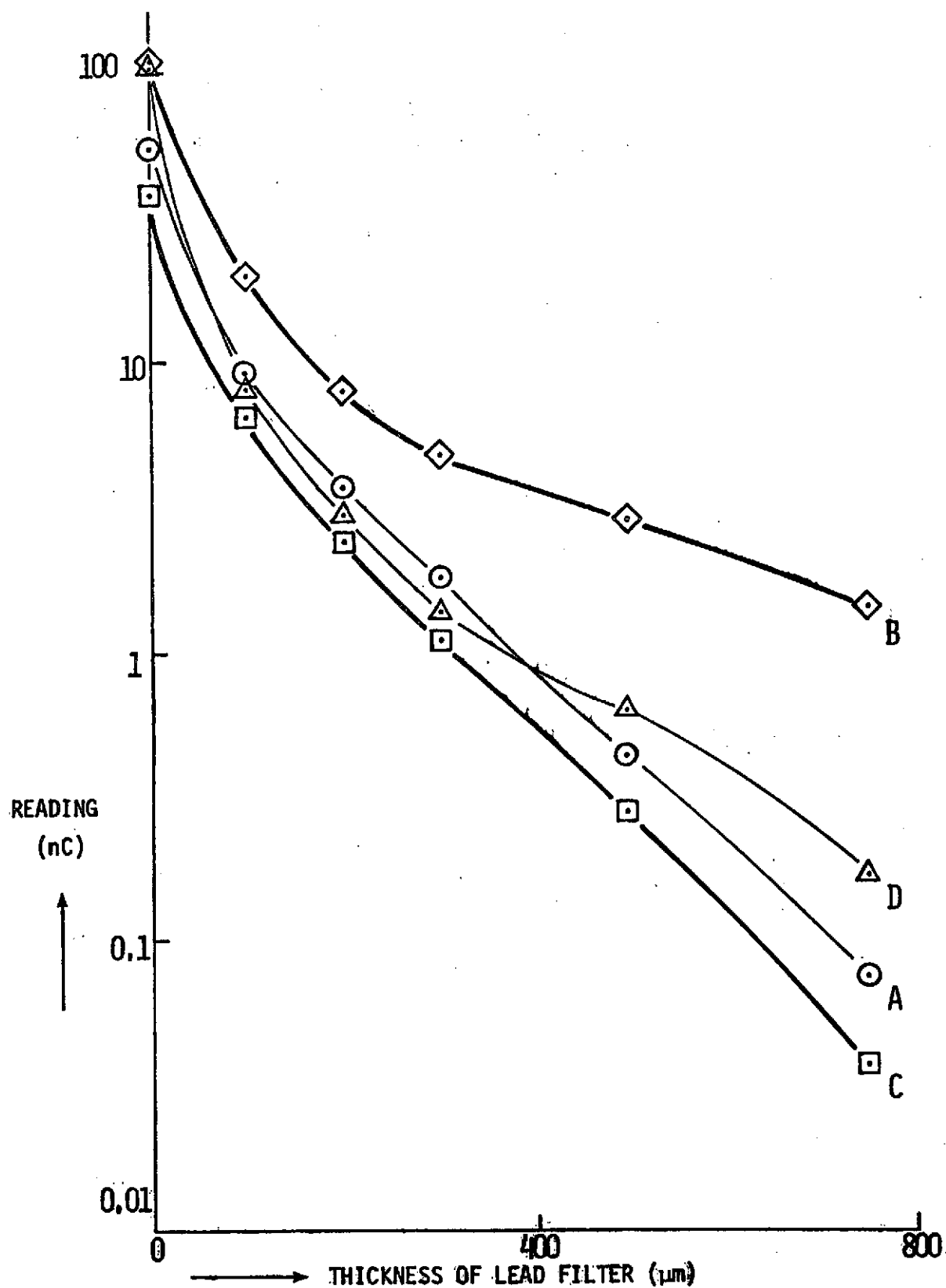


Figure 4. Plot of TLD Readings vs Thickness of Lead Filters, for Sensors at A, B, C, and D. The Values at A, B, and D are the Average of Three Values, all Within About  $\pm 5\%$ .

REPRODUCIBILITY OF THE  
ORIGINAL PAGE IS POOR

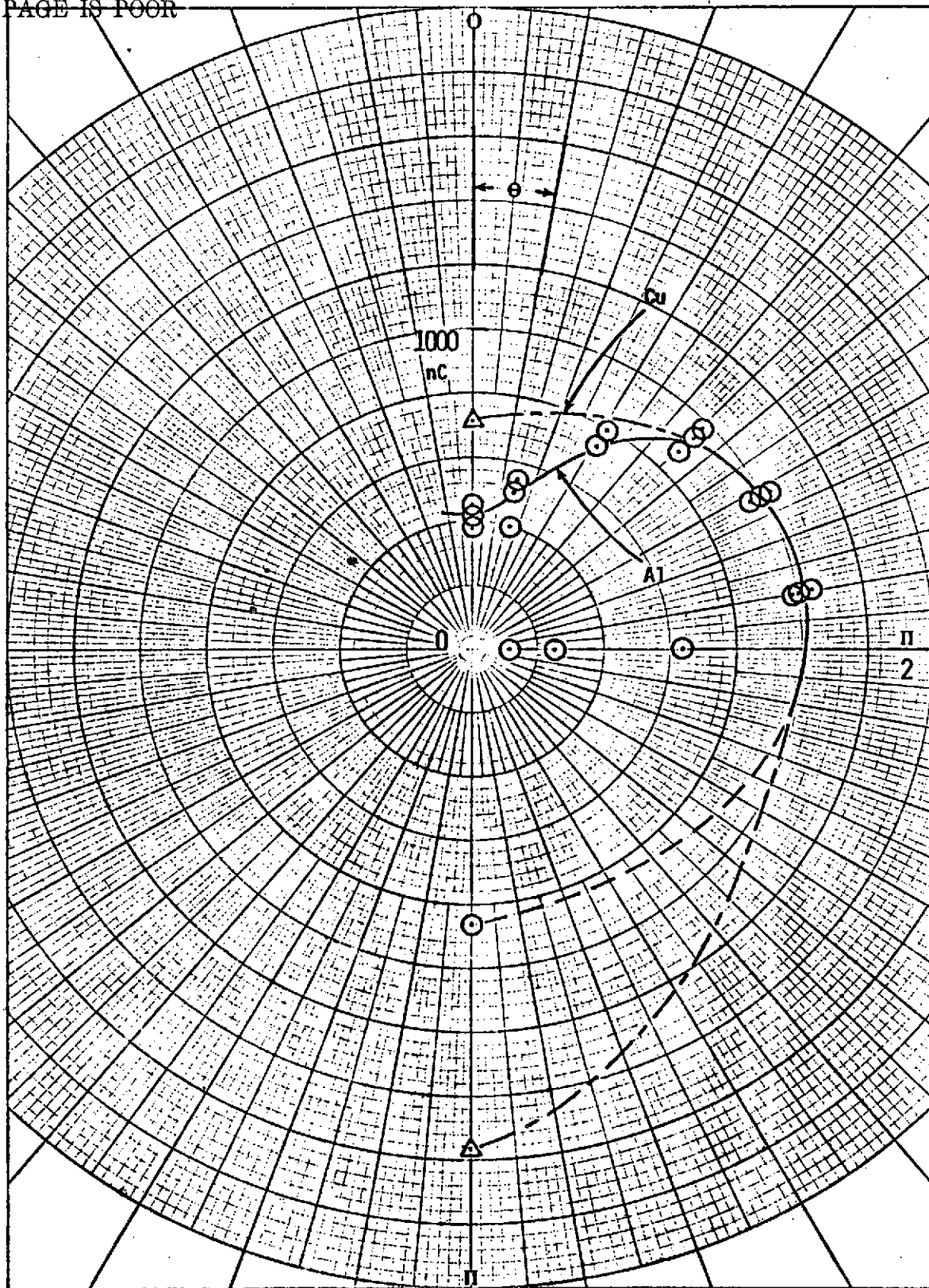


Figure 5(a). Polar Diagram of Medium Energy ( $\approx 20$  keV) X-rays

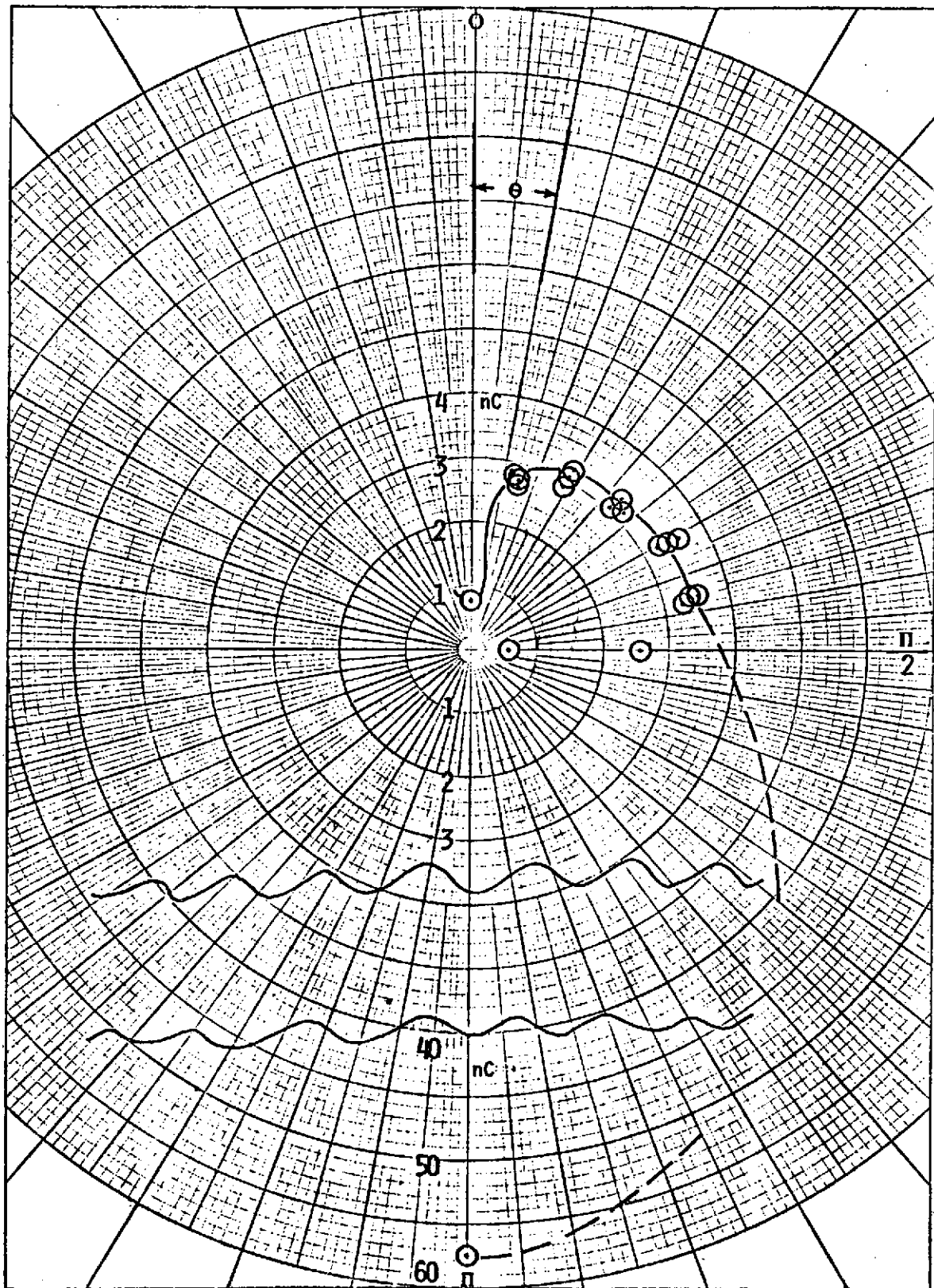
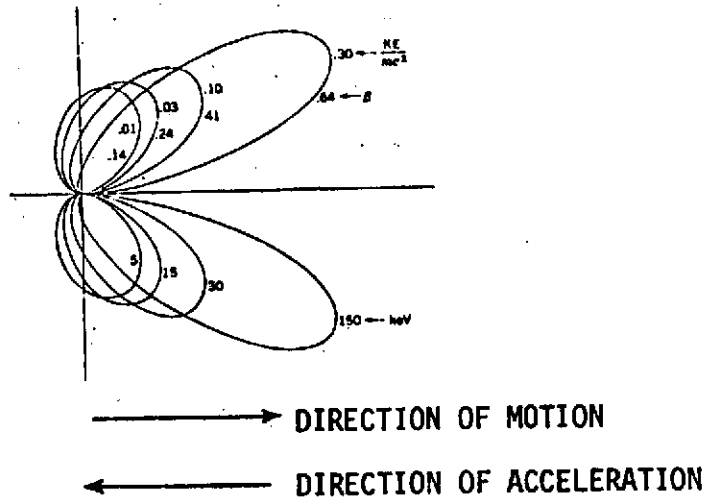


Figure 5(b). Polar Diagram of High Energy ( $\approx 100$  keV) X-rays

(a)



REPRODUCIBILITY OF THE  
ORIGINAL PAGE IS POOR

(b)

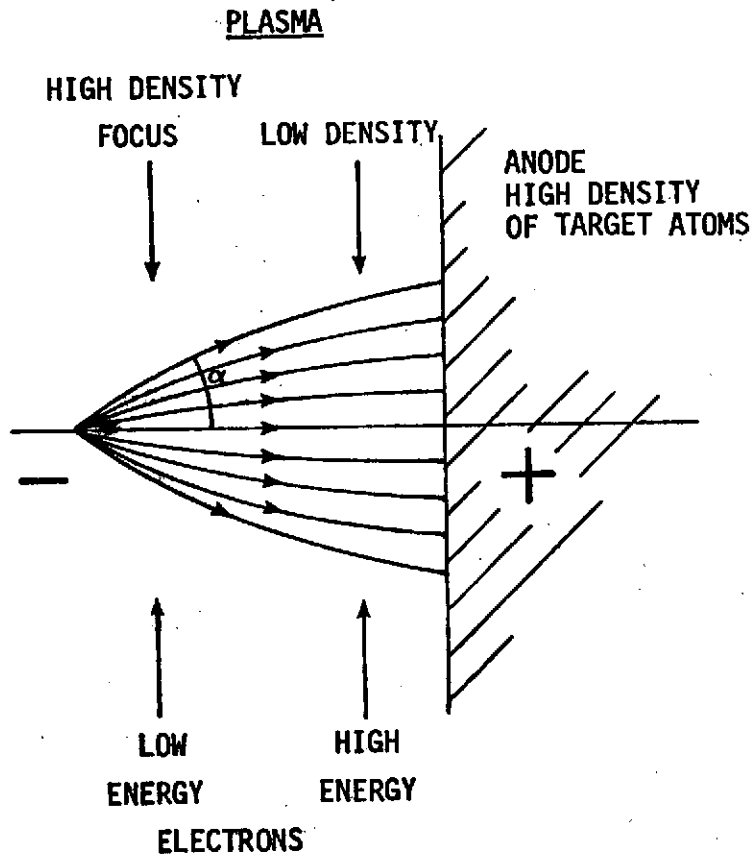


Figure 6. (a) Radiation from a Single Electron  
(b) Qualitative Picture of Electron Trajectories  
Lying in a Cone From A to B



## Appendix D

### SPATIAL DISTRIBUTION OF ELECTRON TEMPERATURE IN A PLASMA FOCUS

#### Summary

The spatial distribution of the electron temperature in a plasma focus was obtained by measuring the intensity of X-rays using filters and thermoluminescent detectors. Rasters of the detectors (9x9) were placed in pinhole cameras and X-ray images of the plasma recorded. Two such rasters irradiated simultaneously through different filters yielded a two dimensional point by point estimate of electron temperature. Values of  $10 \text{ KeV} \pm 1 \text{ KeV}$  were obtained near the anode surface of a plasma focus, falling away rapidly above it.

## Spatial Distribution of Electron Temperature in a Plasma Focus

### I. Introduction

An estimate of the electron temperature in a plasma that emits X-rays can be made by measuring the intensity of radiation transmitted through various filters and taking the ratios of the signals.<sup>(1,2)</sup> Hitherto the values obtained have been averages for the plasma as a whole. In order to understand the mechanism of X-ray emission from a plasma focus, it is of interest to ascertain the spatial distribution of the electron temperature.

The X-ray intensity can be measured using thermoluminescent detectors (TLD)<sup>(3)</sup>, which are small squares of various crystals  $1/8" \times 1/8" \times 1/32"$ . In view of their small size, it is possible to make  $9 \times 9$  rasters of TLD's and by using pinhole cameras, form images of the same plasma on two rasters, through different filters. An estimate of electron temperature can then be obtained as a function of position, by taking ratios point by point.

In Section II an outline is given of how the temperature is obtained. Section III gives the experimental arrangement and results.

### II. Method of Estimating the Electron Temperature

The method of estimating  $T_e$  follows references 1 and 2 and is recalled for convenience, but a different filter material was chosen, namely lead, and also it was assumed the measurements would be made through the aluminum vacuum vessel, 2 mm thick. Lead has a high absorption coefficient, so the filters could be thin, and hence the volume in which an X-ray could be scattered by the absorber was small, and multiple scattering reduced, a factor that would improve the imaging of the X-ray patterns.

We assume the plasma has a Maxwellian distribution of electron velocities and that the free-free emission coefficient is of the form given by Kramers<sup>(4)</sup>

$$I = \text{Const. } n_e n_i Z^2 T_e^{-1/2} \exp(-E/KT_e) \quad (1)$$

Here  $n_e$  and  $n_i$  are the electron and ion densities,  $Z$  is the number of charges on the ions,  $E$  is the X-ray energy,  $K$  is Boltzmann's constant and  $T_e$  the electron temperature of the plasma.

Let the radiation now impinge on a filter whose linear absorption coefficient is  $\mu$  which depends on  $E$  the X-ray energy. For most materials except at the K, L . . . edges

$$\mu(E) = A_n E^{-3} \quad (2)$$

where  $A_n$  is a constant for the material and the subscript depends on whether  $E$  lies above or below the K, L . . . edges. For example for lead, above 89 KeV, the K edge,  $A_1 = 6.35 \times 10^7 \text{ (cm}^{-1}\text{KeV}^3\text{)}$  and if  $E$  is in KeV, then  $\mu$  is in  $\text{cm}^{-1}$ ; from 89 down to 15 KeV  $A_2 = 9.5 \times 10^6$ ; from 15 to 13.1 KeV  $A_3 = 3.94 \times 10^6$ , etc. As the contribution transmitted through the filters below 15 KeV is small, we will use  $A_1$  and  $A_2$  only. For aluminum, the constant  $B_1 = 7.3 \times 10^4$  was used over the above range.

The total intensity transmitted in the energy range  $E_p$  to  $E_q$  for several filters in series is then

$$I = \text{Const } T_e^{-1/2} \int_{E_p}^{E_q} \exp \left[ -E/KT_e - (A_n x_A + B_n x_B + \dots)/E^3 \right] dE \quad (3)$$

where  $A_n, B_n \dots$  are the appropriate constants denoting materials A, B . . . of thickness  $x_A, x_B \dots$ . The total intensity is the sum of such integrals over several energy ranges involving different constants. Eqn(3) was integrated by computer using Simpson's rule, for various temperatures and filters. Six values of  $T_e$  were chosen, namely 3, 5, 10, 15, 20 and 25 KeV,

values encompassing the probable plasma temperature. The different filters were taken as 2 mm Aluminum alone plus four different thicknesses of lead in turn, namely 102, 229, 508 and 762  $\mu$  m. The integrand approaches zero at low and high energies so the range of integration was from 9 to several hundred KeV in steps of 1 KeV. A plot of intensity vs thickness of lead for different values of  $T_e$  is shown in Fig. 1. The ordinate scale is not absolute.

Now if the ratio  $R$  of the signal through one thickness to that of the signal through a different thickness is taken,  $R$  depends strongly on  $T_e$ . From Fig 1, the inverse function  $T_e$  vs  $R$  is plotted in Fig 2 for two different filter combinations, and it can be seen that a fairly accurate value of  $T_e$  can be obtained even if  $R$  is only roughly known.

The use of ratios is advantageous in three respects: (a)  $R$  is independent of the plasma density (see eqn(1)) as  $n_e n_i Z^2$  cancels. (b) it is independent of impurities in the plasma, important for a plasma focus, because with impurities we would replace  $n_e n_i Z^2$  with  $n_e (n_1 Z_1^2 + n_2 Z_2^2 + \dots)$  where  $n_1, n_2, \dots$  are the densities of the variously charged ions of charges  $Z_1, Z_2, \dots$  and the expression cancels (c) taking a ratio precludes an absolute calibration of the readings of the TLD's.

A measurement of  $R$  would, therefore, yield an estimate of  $T_e$  provided the response of the TLD's is independent of energy.

### III. Experimental Method

We first checked the response of the TLD's vs  $E$  by placing eighteen pairs of TLD's one behind the other so that the first of each pair covered the second completely, and sending the same signal through them in series. The emission from the plasma was collimated by lead to be approximately

parallel. If the signals on the first and second TLD were  $S_1$  and  $S_2$  then the fraction of the X-ray energy retained and measured in a TLD is given by  $\eta = 1 - S_2/S_1$ . Values of  $\eta$  were obtained using different filters as above, and  $\eta$  was found to be  $0.49 \pm 0.05$  for aluminum alone, decreasing to  $0.15 \pm 0.06$  for 2 mm aluminum + filters thicker than 200  $\mu\text{m}$ .

The absorbers could be regarded as band pass filters, ranging from 15-25 KeV half width for the aluminum to 50-75 KeV for aluminum + 762  $\mu\text{m}$  of lead (because of the integrand in eqn(3) and assuming  $T_e = 5$  KeV). Hence,  $\eta$  was constant for energies about about 30 KeV, and possibly higher at lower energies.

First, the X-rays from a total of 65 focuses were recorded on TLD's observing the whole plasma through filters and R obtained for conditions A and B in Fig 2. The readings were 37 for A & 8 for B indicating values of  $T_e$  of 9 and 11 KeV respectively assuming  $\eta$  is independent of E. If we assume the reading for aluminum alone was 0.49/0.15 too high,  $T_e$  becomes 16 KeV, an unlikely value. Probably the low energy X-rays were scattered more by the lead behind the detectors to give too high a reading for the rear TLD, and the value of 0.49 for  $\eta$  was erroneous.

The values of  $T_e$  are an "average" for the plasma. To obtain spatial resolution two 9 x 9 rasters were exposed to 25 focuses through pinholes in lead, one observing through the vacuum vessel wall and the other through a filter of 254  $\mu\text{m}$  of lead in addition. Simultaneously the plasma X-rays were photographed by multiple pinhole cameras through similar filters. A DuPont Chronex Lightning X-ray intensifying screen was placed directly in front of the Polaroid ASA 3000 film, to make a contact print. One to one image-to-object ratios were used in all cases. The results were compared

in Figure -3 where the rasters have been slightly enlarged with respect to the film image, and good correspondence is observed. Where a blank reading is shown, the TLD read zero. The values near the top of raster (a) probably arise from scattering of X-rays through small angles by the lead filter, and should be discarded. The highest reading in (a) corresponds to the same point as the highest reading in (b). Although the film shows saturation, numerical estimates can be made from the TLD's, and point by point ratios obtained to estimate  $T_e$  vs position, (in two dimensions). The highest value of  $T_e$  was near the anode surface and about 9 KeV. About 3 mm above,  $T_e$  dropped to about half this value, as it did over a distance of about 0.5 cm horizontally from the center of the anode. It was not possible to estimate  $T_e$  at the location of the focus about 2 cm above the anode as the readings of raster (a) were not reliable, but  $T_e$  was probably much lower than at the anode surface. It should be noted the detectors had a coarse scale, (see the top two readings of (b)) but estimates could still be made of  $T_e$ .

#### IV. Discussion

It is possible that the measurement of TLD efficiency  $\eta$  was erroneous at the lower energy range because of backscatter. A Maxwellian distribution of electron velocities is assumed, but this may not be the case at higher energies. The measured curves of signal intensity from the whole plasma vs lead thickness show good agreement with Fig 1 for  $kT_e = 10$  KeV, but unfortunately other distributions for example a power law or  $E^{-4}$  also show similar behavior, (Fig 1) so we cannot say whether the signals are due to a "non thermal" component of electrons. Nevertheless, the values of  $10 \text{ KeV} \pm 1 \text{ KeV}$  obtained using curves A and B are not unreasonable although higher

than the 5 KeV generally quoted for a plasma focus. The maximum values from the rasters agree with "averages" from the whole plasma because the main contribution to the signal comes from the hottest point.

#### V. Conclusions

The method is capable of discerning the regions of highest "temperature" in a focus, and in giving quantitative estimates. However, whether a Maxwellian distribution of electrons exists is questionable, but if it does, then the highest temperature in a focus is near the center of the anode surface at about 10 KeV. The temperature falls off away from the point dropping to half value over a distance of about 3 mm, above it, and 5 mm horizontally. Estimates of  $T_e$  in the dense plasma focus, some 2 cm above the anode were not possible.

# BIBLIOGRAPHY

1. R. C. Elton and A. D. Anderson, Naval Research Laboratory Report 6541 March 31, 1967.
2. R. C. Elton, Naval Research Laboratory Report 6738, December 11, 1968.
3. See for example J. R. Cameron, N. Suntharalingam and G. N. Kenney "Thermoluminescent Dosimetry" Wisconsin Press, 1968.
4. H. A. Kramers, Phil Mag 46, 836 (1923).



REPRODUCIBILITY OF THE  
ORIGINAL PAGE IS POOR

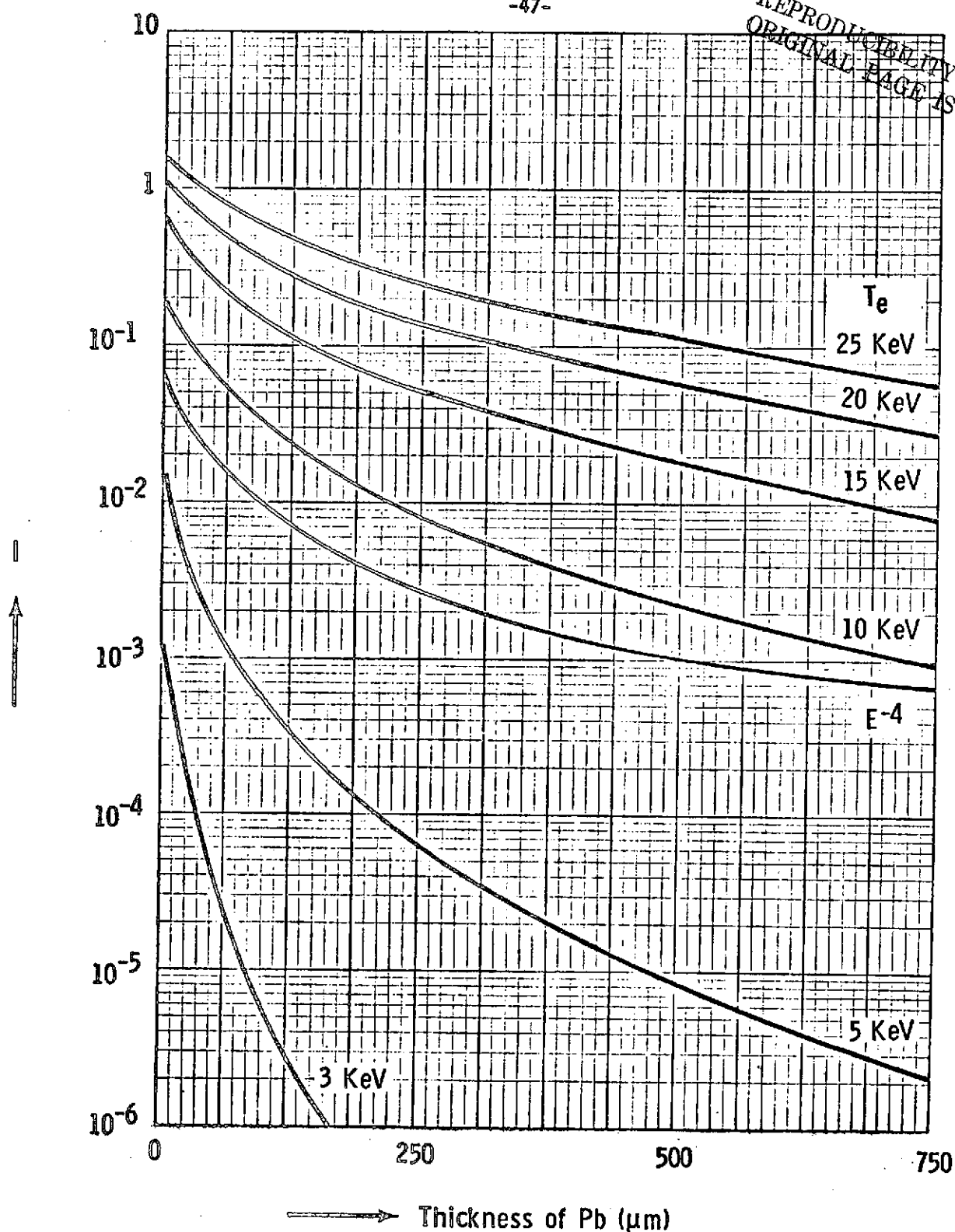


Fig. 1. Transmission of X-rays through 2 mm of aluminum and lead filter as a function of thickness of lead for various plasma temperatures. A power law is shown for comparison. The ordinate scale is not absolute.

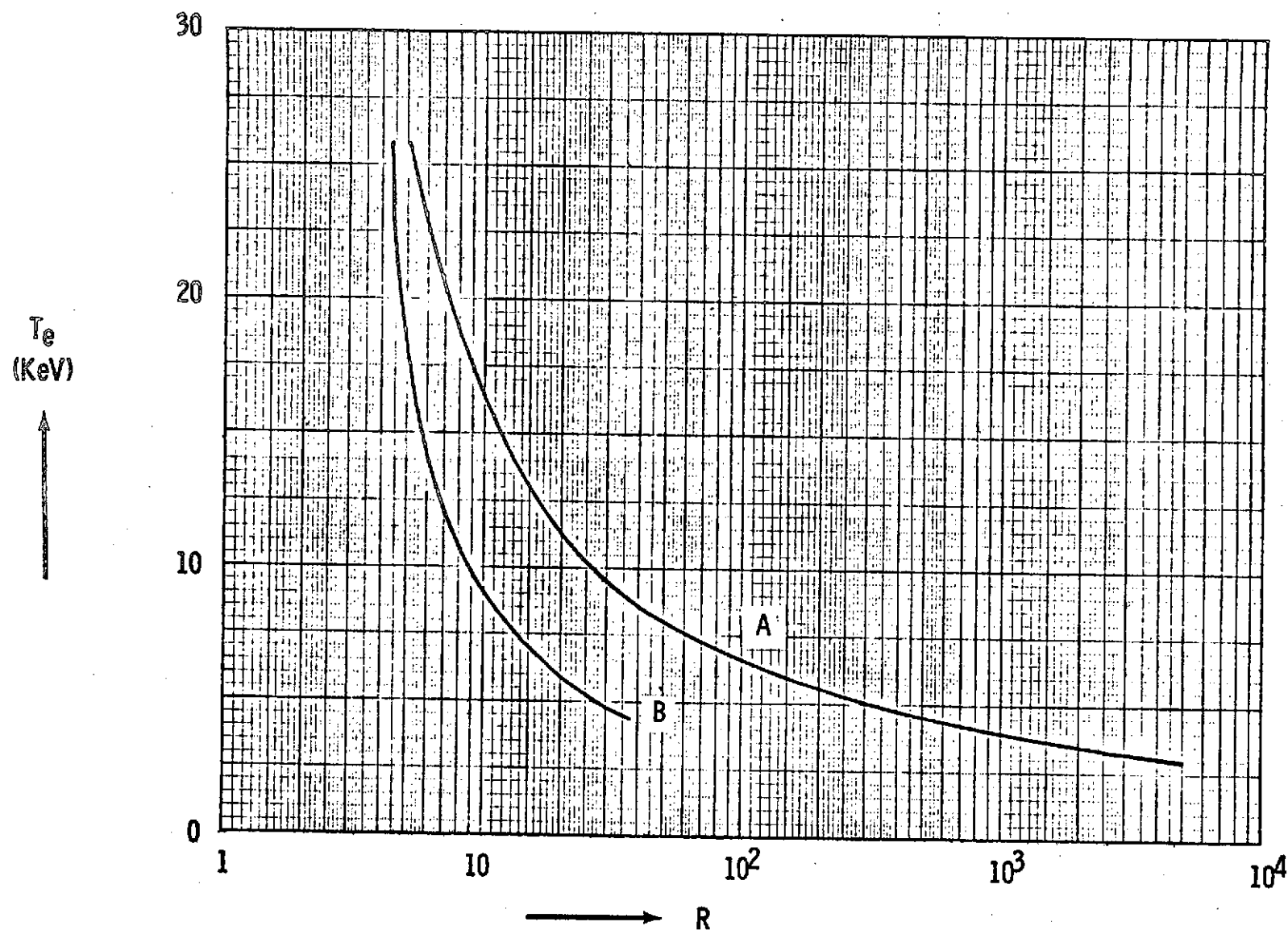
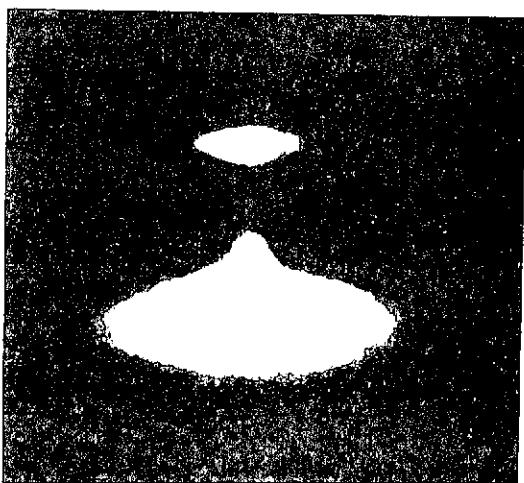


Fig. 2. Plot of  $T_e$  vs  $R$  the ratio of the signals through two different filters: Curve A - signal through 2 mm Al to signal through 2 mm Al and 254  $\mu$ m Pb. Curve B - signal through 2 mm Al and 254  $\mu$ m of Pb to signal through 2 mm Al and 762  $\mu$ m Pb.

(a)



(b)

	2				2	2		
14	9	12	6	3				
						6	5	16
3	4		4	4				
2	2	2	2			3	3	4
3	2				2			
				8	8	6		3
		4	51	83	24			

			3	38				
			76	412				
	2	87	513	843	109	21	3	
413	862	1840	2880	3690	1840	916	440	244
429	800	1220	3270	2800	1500	770	453	253
23	46	69	79	98	72	69	25	15

Fig. 3. Superimposed X-ray pinhole pictures of 25 focuses taken through (a) the 2 mm aluminum vacuum vessel and (b) the vacuum vessel and 254  $\mu\text{m}$  of lead.

## Appendix E

### USE OF ROSS FILTERS TO MEASURE THE ENERGY DISTRIBUTION OF X-RAYS FROM PLASMAS

#### Summary

Ross filters can be used as band pass filters for measurements of X-ray intensity and could in principle, be used to determine the distribution function in energy of X-ray emission from high temperature plasmas. An analysis of the signal to noise problems reveals however that extremely high precision of measurement is required for a thermal plasma. A new method is suggested of designing filters for the energy range 50-100 KeV which appears feasible if the precision is within  $\pm 5\%$ . Such precision is possible with thermoluminescent detectors as sensors.

## USE OF ROSS FILTERS FOR MEASURING THE ENERGY DISTRIBUTION OF X-RAYS FROM PLASMAS

### I. Introduction

Plasma focus devices emit X-rays of energies up to about 500 KeV, as well as neutrons. Previous measurements of the distribution in energy of the X-rays have suggested a power law with the emission proportional to  $E^{-n}$ , with  $n = 4 \pm 1$  for energies over 100 KeV.<sup>(1)</sup>

It is the purpose here to see if it would be possible to make measurements of the X-ray spectra using Ross filters<sup>(2,3)</sup> in the range 5 - 100 KeV. Such filters are useful for observing strong emission lines, and have also been used previously with plasmas to try and estimate electron distribution functions<sup>(4)</sup>. However, in attempting to measure a spectrum, there can be considerably more energy outside the band pass region than within it. The Ross filter technique consists of measuring both contributions, and subtracting two signals to obtain the energy within the band pass region. The question arises of the magnitude of the signals vs the difference between them.

Here the problem of signal to noise, or precision required, is investigated for plasma measurements if thermoluminescent detectors are used as sensors.

### II. Design of Ross Filters.

For convenience, we recall the method of designing a pair of matched filters. Fig 1(a) shows a  $\ln \mu$  vs  $\ln \lambda$  diagram (where  $\mu$  is the linear absorption coefficient in  $\text{cm}^{-1}$ ), for two materials A and B whose K edges at  $\lambda_A$  and  $\lambda_B$  are close together. For most materials  $\mu \propto \lambda^3$  so the slopes are constant. If materials A and B are chosen so that

$$\mu_{A1}/\mu_{A2} = \mu_{B1}/\mu_{B2} \quad (1)$$

then it is possible to make two filters of thickness  $x_A$ ,  $x_B$  such that

$$\mu_{A2} x_A = \mu_{B2} x_B \quad (2)$$

and the  $\ln \mu x$  vs  $\ln \lambda$  curves will coincide except between  $\lambda_A$  and  $\lambda_B$ .

Figure 1(b) shows  $\ln \mu x$  plotted vs  $\ln E$ , the energy, instead of wavelength for a pair of matched filters. If the signals transmitted through two such filters are subtracted, then this is equivalent to a band pass filter with a band width  $E_{KA} - E_{KB} = \Delta E$ .

Thus, the materials are chosen so that  $\Delta E$  is reasonable, and also eqn(1) is obeyed. To find  $x_A$  and  $x_B$ , the criterion usually chosen, which does not seem critical, is to make  $\mu_{B2} x_B$  such as to reduce the transmitted signal to 2/3 of the incident intensity at the low energy end of the band pass, or

$$x_B(\text{cm}) = 0.4055 \mu_{B2}^{-1} \quad (3)$$

and then calculate  $x_A$  from eqn(2). Filter B would then transmit a large signal  $I_L$ , and filter A a smaller signal  $I_S$ , and the difference signal  $I_D = I_L - I_S$  is the signal required. We shall assume the filters perfectly matched.

### III. Precision Required

Suppose that  $I_L$  can only be measured to within an uncertainty  $\pm \Delta I_L$  where  $\Delta I_L / I_L = F$ , typically 0.05. Then to get an accurate value of  $I_D$ , the quantities  $I_S$  and  $I_L$  must satisfy

$$F \ll I_S / I_L \ll 1 - F \quad (4)$$

Both  $I_S$  and  $I_L$  depend on the absorption coefficients of the filters, which can be represented for material A:

$$\mu_A(E) = A_n E^{-3}, \quad A_n = \begin{cases} A_1 ; E > E_{KA} \\ A_2 ; E_{KA} > E > E_{LA} \\ \vdots \end{cases} \quad (5)$$

where  $A_1, A_2$ , etc. are constants and  $E_{KA}, E_{LA} \dots$  represent the energies at the K, L  $\dots$  edges corresponding to material A. The transmitted signal through a filter from an energy interval  $E_p$  to  $E_q$  is then:

$$I_{pq} = \int_{E_p}^{E_q} f(E)T(E) dE \quad (6)$$

where  $f(E)$  is the energy distribution function for the X-rays, and  $T(E)$  is the transmission function  $\exp(-\mu(E)X_A)$  for material A, etc. From Fig 1(b) and eqn(6) the signal  $I$  is the sum of the contributions from the energy ranges AB, BC, and CD, and

$$I_L = I_{AB} + I_{BC} + I_{EF} \quad (7)$$

$$I_S = I_{AB} + I_{DE} + I_{EF} \quad (8)$$

For perfectly matching filters,  $I_D$  depends only on  $I_{BC}$  and  $I_{DE}$ . However,  $I_S/I_L$  depends on  $I_{AB}$  and  $I_{EF}$  in addition.

It can be seen that the energy distribution function affects the precision required. For completeness, it should be mentioned that with a single sharp line, much higher than the background, a rough estimate of an optimizing thickness for maximum  $I_D$  can be obtained by considering an energy distribution function in the form of a single square pulse, with values of zero outside the bandwidth  $E_A$  to  $E_B$ , and an amplitude  $I_0$  (per unit energy) from  $E_A$  to  $E_B$ . From Fig 1(b), it can be seen that  $I_D$  is approximately  $I_0 [\exp(-\mu_{B2}X_B) - \exp(-\mu_{B1}X_B)](E_A - E_B)$  a function of material B only. (as material A is assumed to be matched). For  $I_D$

to be a maximum, an optimum value of  $X_B$  exists,  $X_B = (\mu_{B1} - \mu_{B2})^{-1} \ln(\mu_{B1}/\mu_{B2})$ . The values obtained for  $X_B$  are about one half those from eqn(3) for the filters suitable for the 10 KeV region and approximately equal for the 70 KeV region. For this special case with  $I_{AB} = I_{EF} = 0$  the value of  $I_S/I_L$  has the simple form,  $\mu_{B2}/\mu_{B1}$ , and the problem here is that  $I_S$  can be too small to satisfy the first part of inequality(4).

In contrast with a broad distribution function, it is the second part of the inequality which is difficult to satisfy, i.e., to make  $I_S$  sufficiently different to  $I_L$ . To evaluate the contributions  $I_{AB}$ , etc. eqn(6) must now be integrated presupposing a knowledge of  $f(E)$ . We have taken for the sake of illustration, two possible distribution functions, namely  $\exp(-E/KT_e)$  which follows from Kramer's calculation for the free-free emission coefficient when the electrons are in a Maxwellian velocity distribution at a temperature  $T_e$ <sup>(5)</sup> and secondly a power law or  $f(E) = E^{-4}$ .

A series of six pairs of materials for Ross filters over the range 15 - 100 KeV is quoted in Table I<sup>(6,7)</sup>. The thicknesses of the filters were taken from the literature and agreed with values obtained from eqns (2) and (3) using values of  $\mu$  vs  $\lambda$ <sup>(8)</sup> from known data. Such data also provided values for the constants  $A_n$  in eqn(5). We shall discuss the Titanium - Vanadium, and the Lead-Tantalum pairs, representing the lowest and highest energy ranges, in detail in order to indicate difficulties in the measurement.

A plot of the integrand of eqn(6) is shown in Fig 2, for Titanium and Vanadium where  $f(E) = \exp(-E/KT_e)$ ;  $KT_e = 5$  KeV a reasonable plasma temperature and for three different values of the filter thickness (keeping the same ratio). For titanium,  $A_1 = 4.813 \times 10^5 (\text{cm}^{-1}\text{KeV}^{-3})$  above 4.96 KeV,



the K edge and  $A_2 = 4.098 \times 10^4$  below the K edge; for Vanadium the constant  $B_1 = 6.401 \times 10^5$  above 5.46 KeV and  $B_2 = 5.612 \times 10^4$  below its K edge.

The three sets of thickness shown correspond, one to the literature values, another 10 times thinner and another ten times thicker. The area bounded by the upper and lower branches of any one curve and the two K edge lines corresponds to  $I_D$  and the total area under one curve corresponds to  $I_L$ . As we are considering ratios, the magnitude of the ordinate scale is immaterial, but evidently for all three cases,  $I_S/I_L$  approaches unity to within a few percent, and there will be difficulty in satisfying the right side of inequality(4). The same difficulty occurs for a power law  $E^{-4}$  shown in Fig 3 compared with curve B of Fig 2. We conclude that measurements in the 5 KeV region with a bandwidth of 0.5 KeV would require the signals  $I_L/I_S$  to be measured with a precision of within a few percent.

To measure in the region 67-89 KeV, we consider a Pb-Ta filter and Fig 4 shows  $f(E) T(E)$  for a maxwellian with  $T_e = 5$  and 10 KeV and for  $E^{-4}$ . With curve A a measurement of  $I_D$  would hardly be possible, but it might be possible with curves B and C. The difficulty now is that for a 5 KeV plasma, there are too few X-rays in the high energy tail of the distribution compared with the remainder.

In summary, for the lowest energy and highest energy pair of materials the value  $I_S/I_L$  would be so nearly equal to 1 that very high precision would be required to estimate  $I_D$ .

#### IV. Possible Methods of Improving the Measurements

The signal contribution from any energy range  $E_p$  to  $E_q$  depends on the function of  $f(E) T(E)$  and we expect  $f(E)$  to approach a maxwellian below 100 KeV. Then  $f(E) T(E)$  is of the form  $\exp(-E/KT_e - A_n X_A/E^3)$ . The suggestions for improvement are based on varying  $A_n X_A$  to reduce the energy outside the band pass region relative to the energy within it.

First, examination of Fig. 2 shows that for the Ti-V filters, little can be gained by varying the thickness. Another possibility is to place another material in tandem with the two filters, especially one with a K edge that would reduce the high energy contribution. In which each case,  $A_n X_A$  would be replaced by  $A_n X_A + B_n X_B$  representing materials A and B. A "double filter" consisting of  $1.41 \times 10^{-3}$  cm of Ti and  $1 \times 10^{-3}$  cm of V both covered by V of  $10^{-4}$ ,  $10^{-3}$ , or  $10^{-2}$  cm in turn was evaluated (Fig 5) but the improvement in increasing  $I_D/I_L$  was slight. Another material, Cobalt, with a K edge at 7.71 KeV is also shown. The reduction in signal contribution from above the K edge by the additional material depends on the ratio of its absorption coefficient just above its K edge to that just below, which should be high. Unfortunately, all materials have a ratio of 4 or 5, and it seems little improvement can be achieved where the energy band pass region is centered near  $kT_e$ .

However, in the interesting region of 50-100 KeV, much above  $kT_e$ , a possibility of improvement exists. For the Pb-Ta filter, if the thicknesses are increased to 0.1 cm for both, then a considerable narrowing of the total transmitted energy bandwidth is possible, which results in  $I_D/I_L$  increasing (Fig 6).

To calculate the material thicknesses, eqn(2) is used, but instead of eqn(3), a new criterion is invoked, namely, that  $f(E) T(E)$  should be a maximum at approximately the left edge of the bandwidth, or  $E_{max} = 70$  KeV as in Fig 6. When  $f(E) = \exp(-E/kT_e)$ , then the maximum value of  $f(E) T(E)$  occurs at a value of E

$$E_{max,n} = (3kT_e A_n X)^{1/2} \text{ KeV} \quad (9)$$

with  $kT_e$  in KeV and X the filter thickness in cm. The subscript n shows there can be several maxima corresponding to different values of  $A_n$ ;

however the maxima may not exist if the calculated value of  $E_{\max,n}$  lies outside the energy range where  $A_n$  applies. Thus, eqn(9) shows  $X = 0.12$  cm for  $KT_e = 5$  KeV and 0.06 cm for 10 KeV, so a compromise of 0.1 cm is chosen (An  $E^{-4}$  law gives a maximum at a much smaller value of 0.03 cm).

The additional thickness however causes a reduction in signal but this can be compensated by superimposing many shots on detectors which can store and integrate the information. Such is the case with thermoluminescent detectors (TLD) and measurements show that for 0.1 cm lead, 65 plasma focus discharges produced a signal of about 1000 times greater than the minimum signal that the analyzer could measure. Also TLD's can measure with a precision of better than 5 percent. Hence, measurements with a Pb-Ta, 0.1 cm filter seem feasible.

## V. Conclusions

An analysis of the precision required when using Ross Filter techniques to estimate the spectrum of X-rays from plasmas indicates that such measurements will be difficult, because the two signals which are to be subtracted will be almost equal. In the low energy range ( $<10$  keV, and of order the plasma temperature), the energy within the band pass region is very much smaller than outside it, especially on the high energy side, while in the medium energy range, for example, with a band pass from 67 - 89 keV, the contribution from the tail of a 5 keV plasma is almost negligible. Estimates of the effect of varying thickness or making filters of several materials in series, showed little improvement was possible at low energies. For medium energies, however, considerable improvement may be possible by making thicker filters, and design criteria are given. The decrease in signal strength can be compensated by superimposing many discharges on the detectors.

# BIBLIOGRAPHY

1. J. H. Lee, D. S. Leobbaka and C. E. Roos, Plasma Physics 13, 347(1971).
2. P. A. Ross, Phys Rev 28 425 (1926).
3. P. A. Ross, J. Opt. Soc. Am 16 433 (1928).
4. H. L. L. Van Paassen, R. H. Vandre and R. S. White, Phys Fluids 13 2606 (1970).
5. H. A. Kramers, Phil. Mag. 46, 836 (1923).
6. B. W. Roberts and W. Parrish, Filter and Crystal Monochromator Techniques, "International Tables for X-ray Crystallography" Vol III p. 73, Kynoch Press, Birmingham, England, 1962.
7. D. A. Meskan, H. L. van Paassen and G. G. Comisar, Air Force Report SAMSO-TR-68-50 (1967).
8. H. A. Liebhafsky, H. G. Pfeiffer, E. H. Winslow and P. D. Zerny "Xray Absorption and Emission in Analytical Chemistry", John Wiley 1960 p. 307.

TABLE I  
Ross Filters

Materials A - B	Energy Range (KeV)	Thickness of A		Thickness of B	
		mm	mils	mm	mils
Ti - V	4.96 - 5.46	0.0141	0.555	0.010	0.394
Co - Ni	7.71 - 8.33	0.0108	0.42	0.010	0.38
Mo - Pd	20.00 - 24.34	0.039	1.53	0.0275	1.08
Ag - Sn	25.51 - 29.18	0.0433	1.746	0.052	2.047
Ce - Ta	40.44 - 67.38	0.119	4.605	0.0219	0.862
Ta - Pb	67.38 - 88.04	0.0943	3.713	0.0943	3.713

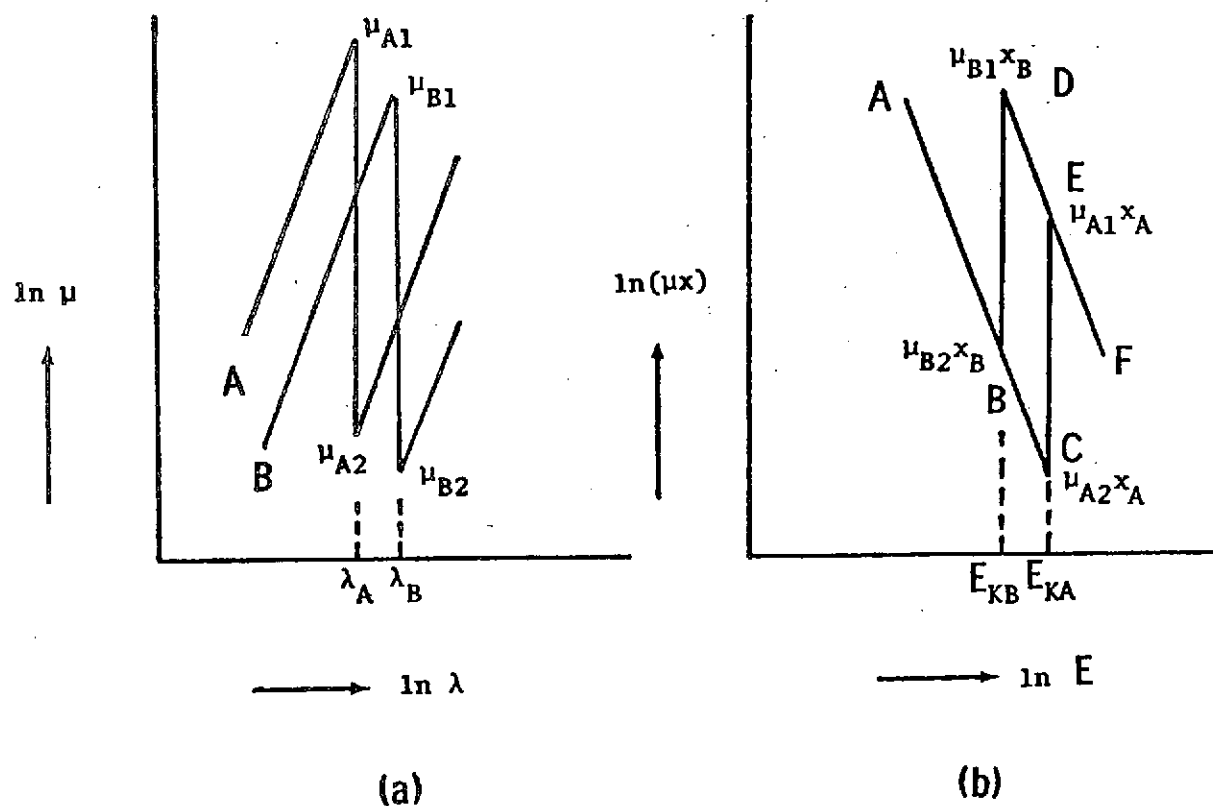


Figure 1. - X-ray absorption coefficients for matched Ross filters.

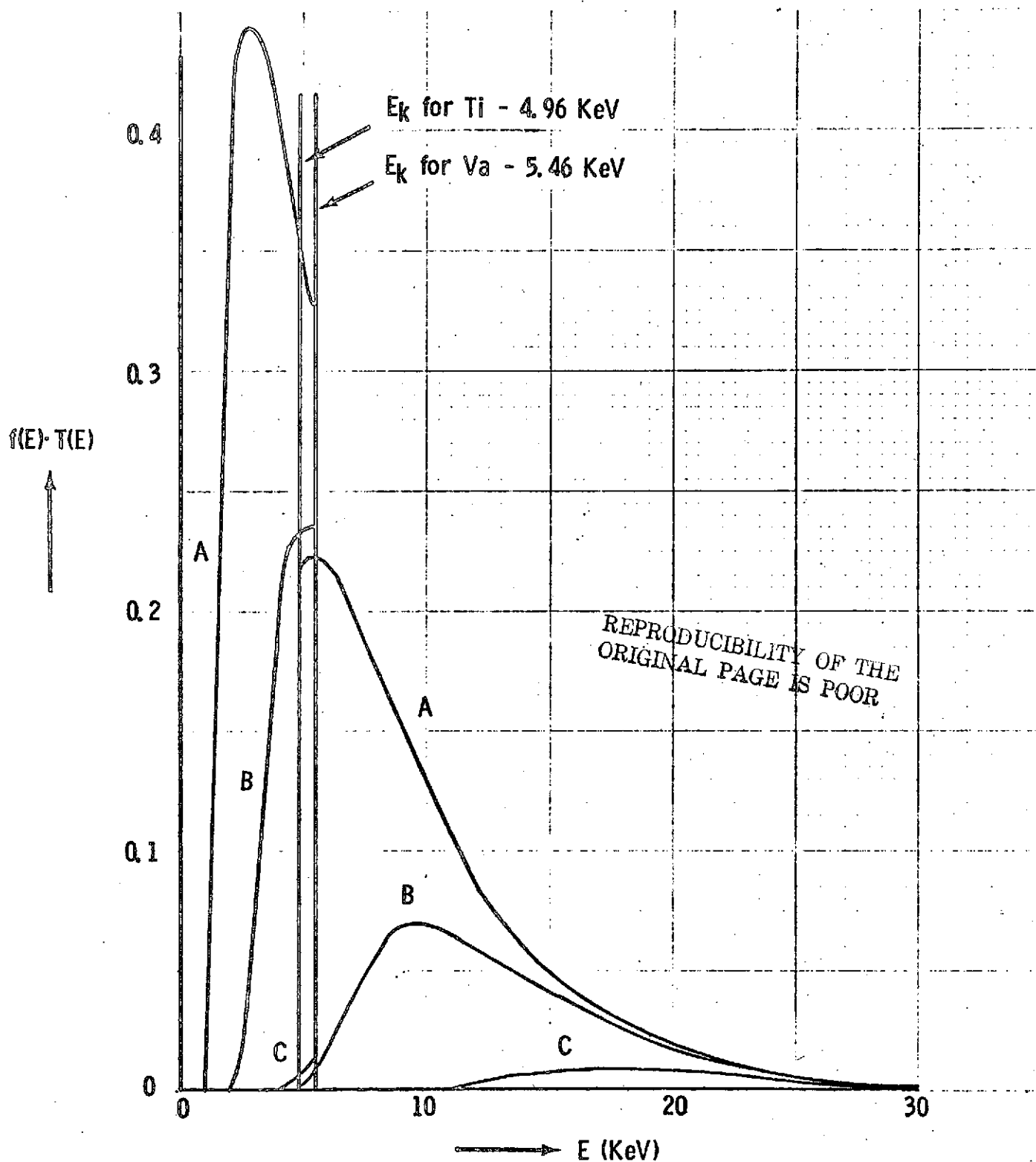


Fig. 2. Plot of  $f(E) \cdot T(E)$  for Ti-V Ross Filters showing effect of thickness. Curve A: Ti -  $1.41 \times 10^{-4}$  cm, V -  $10^{-4}$  cm, curve B: Ti -  $1.41 \times 10^{-3}$  cm, V -  $10^{-3}$  cm, curve C: Ti -  $1.41 \times 10^{-2}$  cm, V -  $10^{-2}$  cm.  $f(E) = \exp(-E/KT_e)$ ;  $KT_e = 5 \text{ KeV}$ .

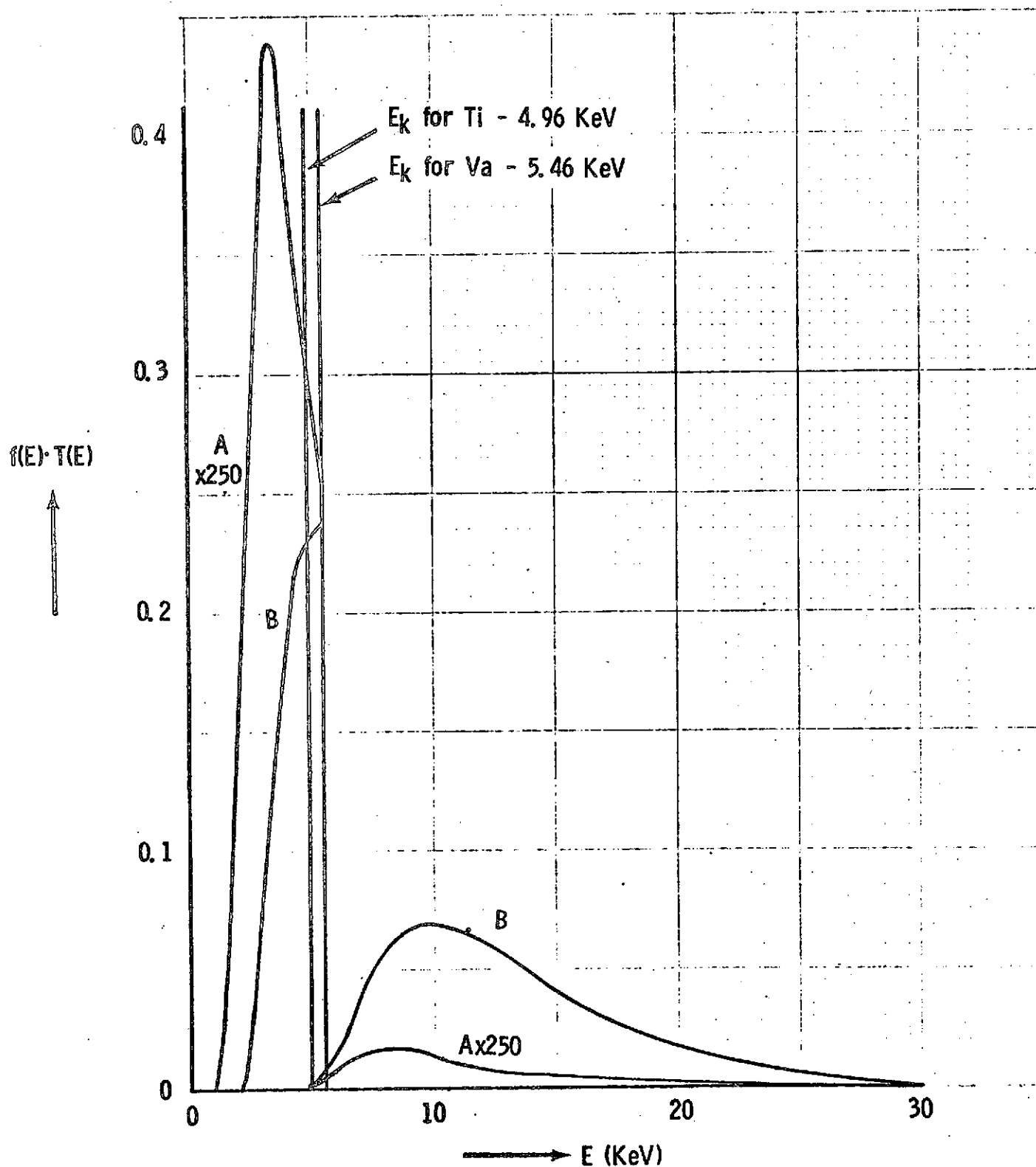


Fig. 3. Plot of  $f(E) \cdot T(E)$  for Ti-V Ross Filters to compare  $f(E)=E^{-4}$  (Curve A) and  $f(E)=\exp(-E/KT_e)$ ;  $KT_e=5$  KeV (Curve B). Thickness of Ti and V respectively -  $1.41 \times 10^{-3}$  cm,  $10^{-3}$  cm.



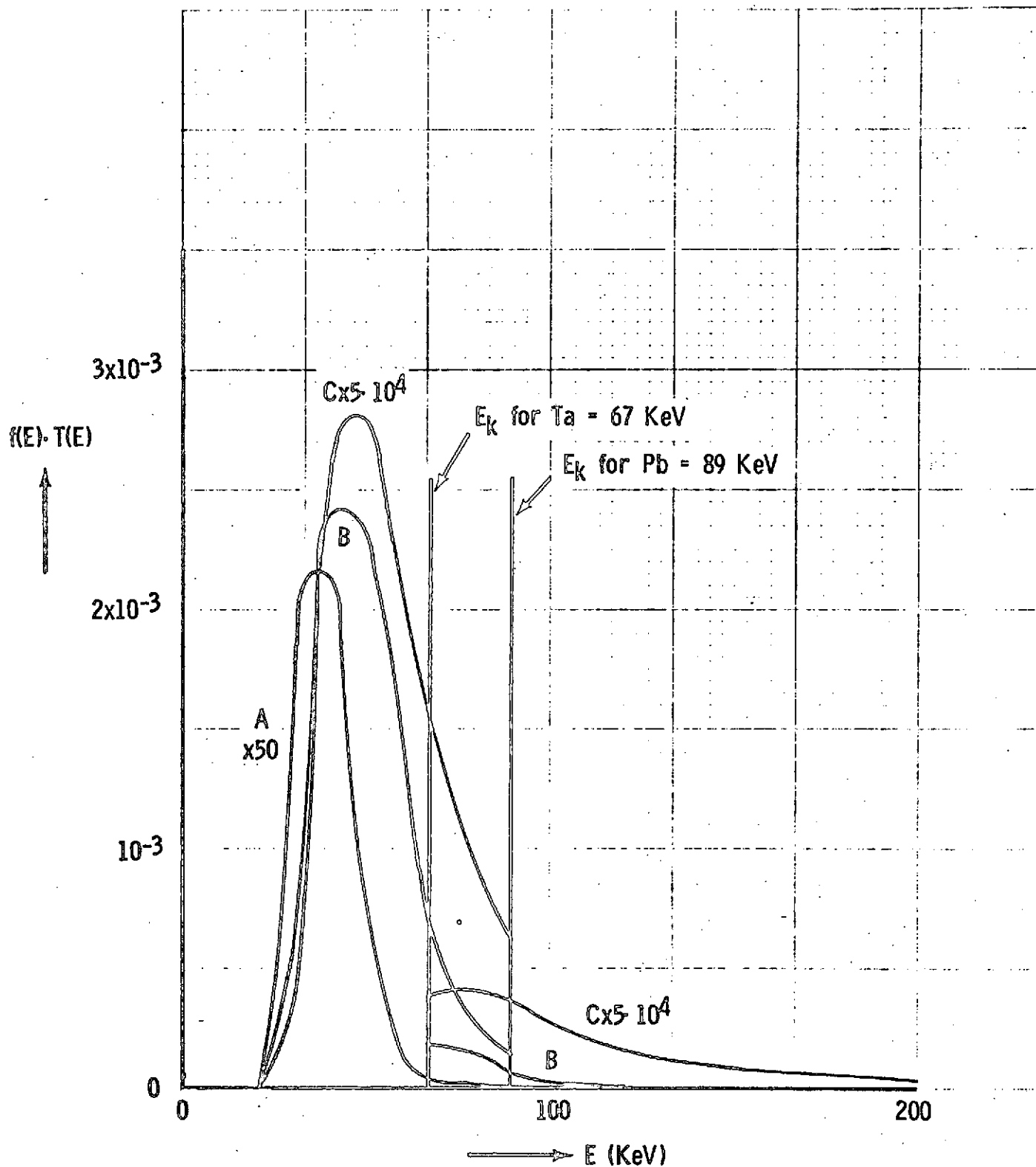


Fig. 4. Plot of  $f(E) \cdot T(E)$  for a Pb-Ta filter to show effect of  $f(E)$ . Curve A:  $f(E) = \exp(-E/KT_e)$ ;  $KT_e = 5$  KeV, curve B:  $f(E) = \exp(-E/KT_e)$ ;  $KT_e = 10$  KeV, curve C:  $f(E) = E^{-4}$ . Thickness of Pb and Ta was 0.01 cm.

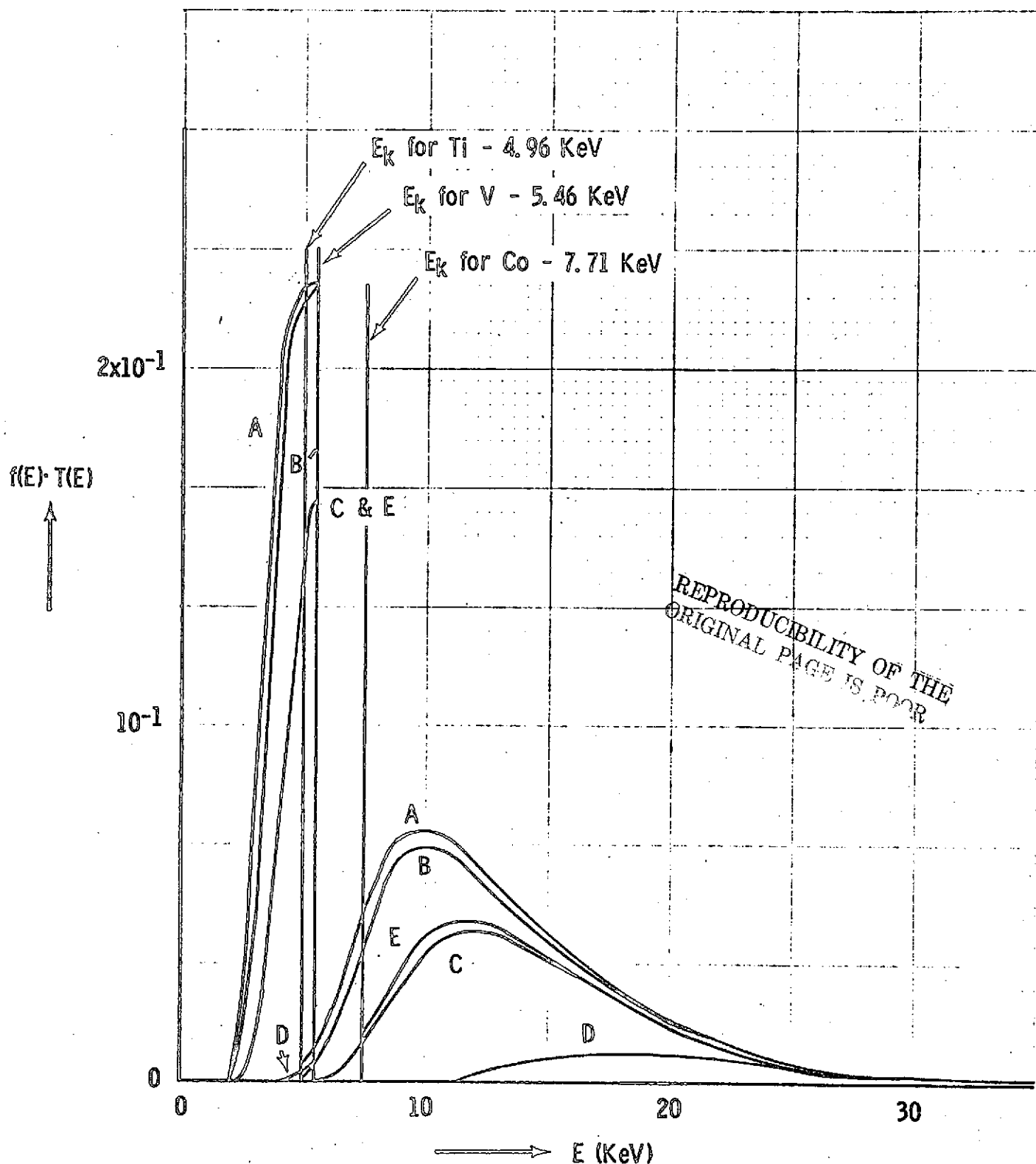


Fig. 5. Plot of  $f(E) \cdot T(E)$  for Ti-V Ross Filters showing effect of additional absorber. Curve A: Ti -  $1.41 \times 10^{-3}$  cm, V -  $10^{-3}$  cm no additional absorber, curve B: with  $10^{-4}$  cm V covering both, curve C: with  $10^{-3}$  cm V, curve D: with  $10^{-2}$  cm V, curve E: with  $3.1 \times 10^{-4}$  cm Co, equivalent to  $10^{-3}$  cm V below 5,46 KeV.  $f(E) = \exp(-E / K T_e)$ ;  $K T_e = 5 \text{ KeV}$ .

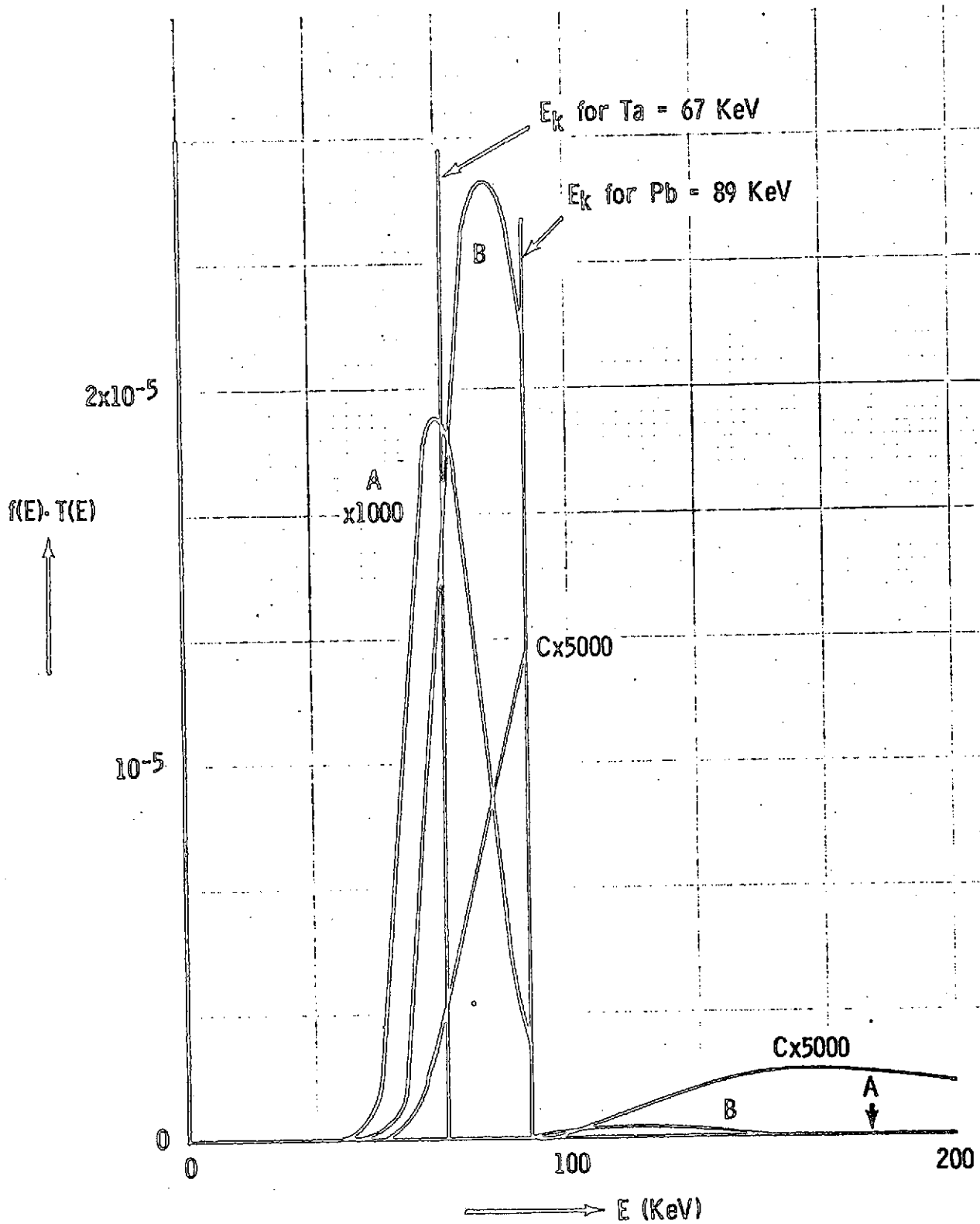


Fig. 6. Plot of  $f(E) \cdot T(E)$  for Pb-Ta thick filters of 0.1 cm each, for different  $f(E)$ . Curve A:  $f(E) = \exp(-E/KT_e)$ ;  $KT_e = 5$  KeV, curve B:  $f(E) = \exp(-E/KT_e)$ ;  $KT_e = 10$  KeV, curve C:  $f(E) = E^{-4}$ .